# Synthesis of Nanoparticles via Solvothermal and Hydrothermal Methods

12

Jianlin Li, Qingliu Wu, and Ji Wu

## Contents



This submission was written by the author(s) acting in his own independent capacity and not on behalf of UT-Battelle, LLC, or its affiliates or successors. All authors make same contribution to this book chapter.

J. Li (✉)
Energy and Transportation Science Division, Oak Ridge National Laboratory, Oak Ridge, TN, USA
e-mail: lij4@ornl.gov

Q. Wu (✉)
Chemical Sciences and Engineering Division, Argonne National Laboratory, Argonne, IL, USA
e-mail: wuq@anl.gov

J. Wu (✉)
Department of Chemistry, Georgia Southern University, Statesboro, GA, USA
e-mail: jwu@georgiasouthern.edu



M. Aliofkhazraei (ed.), *Handbook of Nanoparticles*,
DOI 10.1007/978-3-319-15338-4_17

**Abstract**

This chapter summarizes the synthesis of various types of nanoparticles as well as surface modifications of nanomaterials using hydrothermal and solvothermal methods. First, the definition, history, instrumentation, and mechanism of hydrothermal and solvothermal methods as well as the important parameters affecting the nucleation and crystal growth of nanomaterials are briefly introduced. Then, the specific hydrothermal and solvothermal methods used to grow oxides; Groups II–VI, III–V, and IV; transitional metals; and metal-organic framework nanoparticles are summarized. Finally, the hydrothermal and solvothermal strategies used for the surface modification of nanomaterials are discussed.

**Keywords**

Hydrothermal • Solvothermal • Nanoparticles • Surface modification • II–VI • VI • III–V • Transitional metals • Metal-organic framework • Oxides • Nucleation • Crystal growth

**List of Abbreviations**

| | |
|---|---|
| AC | Acetone |
| BDC | Terephthalic acid |
| CTAB | Cetyltrimethylammonium bromide |
| HKF | Helgeson-Kirkham-Flowers |
| HMDS | Hexamethyldisiloxane |
| MOF | Metal-organic framework |
| NC | Nanocrystal |
| NP | Nanoparticle |
| PFTE | Polytetrafluoroethylene |
| PVP | Polyvinylpyrrolidone |
| SEM | Scanning electron microscope |
| SAED | Selected-area electron diffraction |
| TEM | Transmission electron microscope |
| XRD | X-ray diffraction |

## Introduction

### Definition of Hydrothermal/Solvothermal Process

The term "hydrothermal/solvothermal process" is defined as performing chemical reactions in solvents contained in sealed vessels in which the temperature of solvents can be brought to around their critical points via heating concurrently with autogenous pressures [1]. The process is referred to as "hydrothermal" when water is used as the solvent. In some cases, this term is also used to describe processes conducted at ambient conditions. For the sake of clarification, the approach involving water as the solvent in the hydrothermal process is specifically referred to in this chapter; the term "solvothermal process" is used when organics

are used as solvents. The following terms are commonly used when describing solvothermal/hydrothermal processes:

- Precursors: reactants in forms of solutions, gels, and/or suspensions
- Mineralizers: inorganic or organic additives with high concentrations (e.g., 10 M) to control the pH of solutions
- Additives: organics or inorganics in relatively low concentrations, added to promote particle dispersion or to control crystal morphology

## A Brief History of the Hydrothermal/Solvothermal Technique

The emergence and development of the solvothermal/hydrothermal process is closely linked to the development of nanomaterials. The first report about the hydrothermal process could be traced back to the middle of the nineteenth century, when it was employed to prepare submicrometer- to nanometer-sized quartz particles [2]. However, the research and application of the hydrothermal process in material synthesis lagged from 1840s to the early 1990s because techniques to characterize nanoscale products were not available and, to some extent, because knowledge of hydrothermal solution chemistry was insufficient to successfully realize the control of crystal growth [3]. Hydrothermal techniques revived in 1990s along with the revolution in nanoscale materials and the emergence of high-resolution microscopes from 1980s [4]. Simultaneously, great progress was achieved in understanding chemical and physical properties of hydrothermal systems, which led to development of the solvothermal process, in which organics were introduced as solvents in manufacturing well-controlled nanomaterials [5–8]. In the twenty-first century, the hydrothermal/solvothermal process has gained great successes in manufacturing nanomaterials with crystallinity, crystal phase, morphology, and size control, due to its outstanding advantages, including low process temperature, performance of reactions in liquid environments, low energy consumption, and environmental benignity [9, 10–18].

## Instruments Used in Hydrothermal/Solvothermal Processes

Most hydrothermal/solvothermal reactions proceed in a sealed reactor, known as an autoclave, a pressure vessel, or a high-pressure bomb. In most cases, hydrothermal/solvothermal reactors are metal autoclaves with Teflon or alloy linings or containing an extra can, beaker, or tube made of Teflon, platinum, gold, or silver to protect the autoclave body from the highly corrosive solvent, which is held at high temperature and pressure. In some cases, a Bourdon gauge is fixed to the autoclaves to directly monitor the pressure, and the autoclaves are equipped with stirring accessories to minimize the concentration gradient inside them. In addition, an ideal hydrothermal/solvothermal autoclave should be easy to assembly/disassembly, as well as be leak-proof and possess sufficient running life within the

**Fig. 1** A general-purpose hydrothermal autoclave. The hydrothermal reactions occur inside the Teflon container (Reproduced with permission from Byrappa and Adschiri [3]. Copyright 2007, Elsevier)

**Table 1** The most commonly used reactors for hydrothermal/solvothermal processes[a]

| Type | Temperature (°C) | Pressure (bar) |
|---|---|---|
| Quartz tube | 250 | 6 |
| Cone closure | 750 to ~1,150 | 4,000 to ~13,000 |
| Welded closure | 400 | 3,000 |
| Modified Bridgman autoclave | 500 | 3,700 |
| Piston cylinder | 1,000 | 40,000 |
| Opposed diamond anvil | >2,000 | 500,000 |

[a]Note: Partially adopted from Byrappa and Yoshimura [1]. The work conditions might vary and depend on materials and reaction solutions

experimental temperature and pressure range. Figure 1 shows the most popular general-purpose autoclave used in laboratories. The reactors commonly used in hydrothermal/solvothermal processes are listed with their initially designed operating temperatures and pressures in Table 1. The working conditions of autoclaves vary for different materials, including glass, quartz, and high-strength alloys. Temperature, pressure, and corrosive resistance of reactor materials are the most important parameters for the reactor selection. For safety, pressures generated in a sealed vessel should always be estimated and controlled below the strength of autoclave materials.

## Fundamental Mechanisms of Crystal Growth via the Hydrothermal/Solvothermal Process

Material synthesis through hydrothermal/solvothermal methods is a crystallization process directly from solutions that usually involve two steps: crystal nucleation

and subsequent growth. By controlling processing variables, such as temperature, pH, reactant concentrations, and additives, the final products could be fabricated with desired particle sizes and morphologies. The phenomena underlying the size and morphology control through tuning the process variables are the overall nucleation and growth rates, which depend on supersaturation [19]. The term supersaturation is defined as the ratio of the actual concentration to the saturation concentration of the species in the solution [20]. Although the presence of myriad species in the hydrothermal/solvothermal solution makes it difficult to determine the exact reaction equilibria, several thermodynamic models have been established to calculate the solubility of the species that exist in hydrothermal/solvothermal systems, especially in aqueous solutions [3, 21–26]. For instance, Shock and coworkers proposed a revised Helgeson-Kirkham-Flowers (HKF) model [8], and the solubilities of hundreds of inorganic compounds in aqueous solution have been calculated over wide ranges of conditions (25–1,000 °C, 0.1–500 MPa) based on the HKF model [5–8]. Other researchers subsequently proposed further revised HKF models to calculate the solubility more precisely [27–30]. From the revised HKF model, the equilibrium constant K of species in solution could be calculated as follows (Eq. 1) [30]:

$$\ln K_{T,\rho} = \ln K_{T_r,\rho_r} - \frac{\Delta H^0_{T,\rho_r} + \beta(1-\rho^*)^{\frac{2}{3}} + \alpha\Delta\omega_{T_r,\rho_r}T_r}{R} \times \left(\frac{1}{T} - \frac{1}{T_r}\right) - \frac{\Delta\omega_{T,\rho}}{RT}\left(\frac{1}{\varepsilon} - 1\right) + \frac{\Delta\omega_{T_r,\rho_r}}{RT}\left(\frac{1}{\varepsilon_{T_r,\rho_r}} - 1\right) \quad (1)$$

where $\rho^*$ is a density ratio of water (density at actual conditions/density at reference conditions (25 °C and 0.1 MPa)); $\alpha$ is a constant, $6.385 \times 10^{-5}$ $K^{-1}$; $\varepsilon$ is the dielectric constant of water; $\omega$ is the parameter determined by reaction system; the subscript "$r$" refers to the reference state; and $\beta$ is a reaction-dependent constant.

The reaction-dependent constant is determined as follows (Eq. 2):

$$\beta = \lambda_1\left(\Delta C^0_{P,T_r,\rho_r} + \lambda_2\Delta\omega_{T_r,\rho_r}\right) + \lambda_3 \quad (2)$$

where $\Delta C^0_{P,T_r,\rho_r}$ is the heat capacity. $\lambda_1$, $\lambda_2$, and $\lambda_3$ are 97.66 K, $2 \times 10^{-4}$ $K^{-1}$, and $-3.317 \times 10^2$ J $mol^{-1}$, respectively. It is obvious from the above equations that the solubility of species in solution strongly depends on the properties of the solvents, including their density and dielectric constant (the dielectric constant is discussed further in section "The Effect of Other Factors").

Nucleation occurs when the solubility of the solute exceeds its limit in the solution (i.e., when the solution becomes supersaturated). The reaction is irreversible; the solute precipitates into clusters of crystals that can grow to macroscopic size [31]. Following nucleation, the crystals grow sequentially or concurrently via a series of processes involving the incorporation of growth units, which have the same composition as crystal entities but possess the same or different structures,

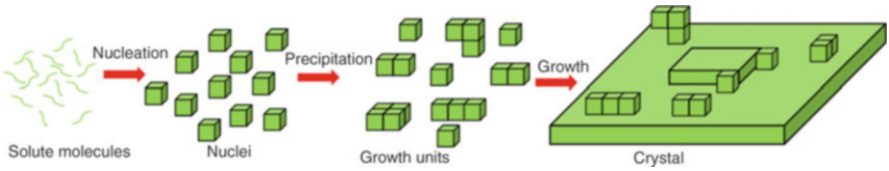


**Fig. 2** Schematic representation of crystal growth mechanism under the hydrothermal/solvothermal environment

from the bulk solution into the existing crystal entities and causing increased sizes. These different processes can be roughly categorized into four steps: transport of units through solution, attachment of units to the surface, movement of units on the surface, and attachment of units to growth sites. The schematic representation of widely recognized mechanisms of crystal growth via hydrothermal/solvothermal methods is shown in Fig. 2. However, there are a lot of debates on the crystal growth mechanisms under hydrothermal/solvothermal conditions, including identifying the growth unit attached to the surface of crystal entities and controlling steps in the crystal growth process. For instance, Schoeman proposed that the growth unit of a zeolite crystal was probably an anionic silicate species, most likely a monomer [32]. Other researchers have proposed that it is also possible that nanoparticles (NPs) are also growth units of zeolite crystal under hydrothermal conditions [33, 34]. To contribute to crystal growth, each growth unit would require its own sequence of governing steps.

As an abundant, low-toxic liquid with a high dielectric constant, water is the most widely used solvent in the hydrothermal/solvothermal process, and hydrothermal chemistry has been widely investigated. The critical temperature and pressure of water are 374 °C and 22.1 MPa, respectively. The properties of water vary with the temperature and pressure, especially above the critical point. For instance, as shown in Fig. 3, the dielectric constant of water is 78 at room temperature, which is favorable for the dissolution of polar salts. With increasing temperature and decreasing pressure, the dielectric constant of water decreases to ~10 in the critical region and above the critical point drops dramatically to between 2 and 10 [35]. According to Eq. 1, the dramatic change in the dielectric constant results in a remarkably reduced solubility of solute species, leading to high supersaturation in the solution, and thus facilitates the nucleation growth of crystals. From another aspect, the low dielectric constant allows the dissolution of organic species in the supercritical water, where they act as additives to control the crystal nucleation and growth. Similar trends could also be observed for solvothermal solution systems.

Nonaqueous organics have also been widely utilized as solvents in the solvothermal fabrication process, which is analogous to the hydrothermal process. The organic solvents commonly used in solvothermal processes include methanol [36], 1,4-butanediol [37], toluene [38], and amines [39]. Their physicochemical properties are summarized in Table 2. As an alternative to the hydrothermal process,

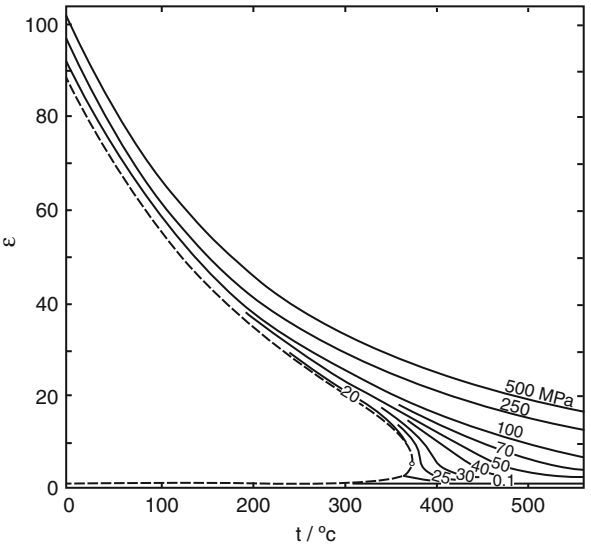


**Fig. 3** The static dielectric constant of water as function of temperature with various pressures (Reproduced with permission from Uematsu and Franck [35]. Copyright 1981, American Institute of Physics)

**Table 2** Properties of commonly used hydrothermal/solvothermal solvents

| Solvent | Formula | Critical temperature (°C) | Critical pressure (MPa) | References |
|---|---|---|---|---|
| water | $H_2O$ | 374 | 22.1 | [35] |
| Ethylenediamine | $H_2NCH_2CH_2NH_2$ | 319.9 | 62.1 | [40] |
| Methanol | $CH_3OH$ | 239.2 | 8.1 | [41] |
| Ethanol | $CH_3CH_2OH$ | 241.1 | 6.1 | [41] |
| Toluene | $C_7H_8$ | 320.6 | 4.2 | [42] |
| Ethanolamine | $HOCH_2CH_2NH_2$ | 398.25 | 8 | [43] |

the solvothermal process can make the reactions occur at relatively low temperatures and pressures, and most importantly, the solvothermal process can handle precursors that are sensitive to water [44]. In addition, the products derived from the solvothermal process are free from foreign anions [45, 46], and morphology [47] or crystal phase control [48] is easily realized.

## The Effect of Other Factors

Several other factors can significantly affect the crystal nucleation and growth of nanomaterials during hydro-/solvothermal syntheses, such as additives [49], precursors [50, 51], reaction time [52], and filling factor (the ratio of the volume filled with solution to the total reactor volume) [53].

The evolution of hydrothermal/solvothermal technique has been briefly summarized in Table 3.

**Table 3** The brief summary of hydrothermal/solvothermal technique

| Time | Research highlights | Typical equipment | Representative references |
|---|---|---|---|
| 1845–1950 | Mineral synthesis (especially quartz with large size and high yields), natural conditions mimic | Morey autoclaves, flat closures, welded closure | [54–58] |
| 1950–1980 | Phase diagrams of aqueous systems with high-temperature and pressure, novel, and advanced materials | Autoclaves with improved sealing: Tuttle-Roy, welded closures, modified Bridgman | [59–69] |
| 1980–1990 | Material sciences, advanced ceramic powders, physical chemistry of hydrothermal solutions | General autoclaves with Teflon or alloy linings | [9, 70–81] |
| >1990 | Engineering of hydrothermal process, emergence of solvothermal | Diverse reactors designed for specific requirements, such as batch reactors, flow reactors | [22, 82–103] |

## Synthesis of Nanomaterials via Hydrothermal and Solvothermal Methods

Nanostructured materials with controllable size, shape, crystallinity, and tunable surface functionalities have attracted extensive research attention due to their unique optical, electronic, magnetic, mechanical, and chemical properties, which are derived mainly from the quantum confinement effect and large surface-to-volume ratios. The hydrothermal and solvothermal synthetic methods are considered to be among the most promising approaches to preparing nanomaterials. These methods possess many advantages, such as producing a large amount of nanomaterials at a relatively low cost and yielding highly crystalline nanocrystals (NCs) with well-controlled dimensions. Hydrothermal and solvothermal methods can be combined with microwaves and magnetic fields for semicontinuous synthesis of materials having much improved reproducibility and high quality. In this section, the hydrothermal and solvothermal methods employed to prepare oxides; Group II–VI, III–V, and IV NPs; metal-organic frameworks (MOFs); and transitional-metal NPs will be described and summarized.

### Metal Oxides Nanoparticles

Nanostructured metal oxides are attractive materials that, because of their unique properties, are widely applied in catalytic, ceramic, electrical, optical, and other fields. The properties of metal oxides directly determine their practical applications. Compared with the hydrothermal process, the solvothermal process could produce metal oxides that are smaller and have a narrower size distribution, and they could

be produced at a lower temperature [44]. Extensive work has been reported in the preparation of numerous nanostructured metal oxides, such as $Al_2O_3$, CuO, $Fe_2O_3$, NiO, $ZrO_2$, $TiO_2$, $BaTiO_3$, and $SrTiO_3$, through both hydrothermal and solvothermal processes [19, 104–112]. Common metal oxides obtained through those processes are summarized in Tables 4 and 5. $TiO_2$ is selected as a representative binary metal oxide to demonstrate the effect of the hydrothermal/solvothermal process on the properties of metal oxides. These properties include the crystallinity, crystal phase, morphology, and particle size, which crucially determine the further applications of final metal oxides.

Extensive studies have been made to prepare nanostructured $TiO_2$ through hydrothermal/solvothermal processes. Formation of $TiO_2$ goes through two steps regardless of the solvents used: (1) the formation of titanium hydroxides via a hydrolysis reaction and (2) the formation of titania via a dehydration/condensation reaction. The hydrolysis and condensation reactions might take place in series in a highly diluted solution. However, it is quite difficult to separate these two reactions in a concentrated solution. The condensation reaction inevitably occurs with excessive $OH^-$ groups [126], leading to the formation of clusters, polymers, or NCs of titania. These clusters are the embryos of titania crystals that can further grow into large particles during the subsequent heat treatment [112]. The properties of the final titania products can be tuned via adjusting the processing parameters.

The presence of a mineralizer is one of these important parameters. $HNO_3$ has been reported to be a better mineralizer in the hydrothermal process to obtain monodispersed NPs with homogeneous composition than NaOH, KOH, HCl, HCOOH, or $H_2SO_4$ [127]. The mineralizer concentration also greatly affects the phase and morphology of hydrothermal titania products. Under hydrothermal conditions, the phase and morphology of titania will transfer from rutile nanorods to anatase NPs, brookite nanoflowers, dititanate nanosheets, and trititanate nanoribbons sequentially, as the pH is varied from highly acidic (6 M HCl) to highly alkaline (10 M NaOH) [128] or KOH [129], with tetrabutyl titanate or $TiCl_4$ being used as the precursor.

When titania powders are the precursors and NaOH is the mineralizer, only sodium titanate nanotubes could be produced; increasing the concentration of NaOH can further enhance the nanotube to unreacted titania particle ratio [130, 131]. Interestingly, after ion-exchange treatment of the sodium titanate nanotubes, the H-titanate nanotubes are transformed to anatase NPs with rhombic shape when the $pH > 1$ and turned into rutile nanorods with two pyramidal ends when the $pH < 0.5$ [131].

Another crucial factor is solvent. Water is the solvent in the hydrothermal process and usually incorporates into the resultant titania product. However, the hydroxyl contents from a water-based ambient condition could be eliminated by replacing the water with organic solvents [132]. In addition, it could be easy to control phase and morphology by merely adjusting the ratio of Ti precursors and organic solvents. For instance, a low $TiCl_4$/acetone (AC) ratio (<1/15) led to anatase $TiO_2$ NCs, and a high $TiCl_4$/AC ratio (>1/10) resulted in rutile $TiO_2$ nanofibers when $TiCl_4$ was the precursor and AC was the solvent used in a solvothermal process (Fig. 4) [133]. The employment of organic

**Table 4** Representative binary metal oxides obtained through hydrothermal/solvothermal process

| Compound | Starting materials | Solvent | Particles size | Morphology | References |
|---|---|---|---|---|---|
| $TiO_2$ | $TiO_2$ nanopowder, NaOH (15 M[a]) | $H_2O$ | 30–80 nm in diameter | Nanowire | [113] |
| $MnO_2$ | $MnSO_4 \bullet H_2O$, $(NH_4)_2S_2O_8$ | $H_2O$ | 5–20 nm in diameter, 2.5–4 μm in length | Nanowire | [92] |
| $CeO_2$ | Hydrated cerium chloride, octadecylamine, ethylenediamine | $H_2O$ + ethanol | 40–50 nm in diameter, 0.3–2 μm in length | Nanorod | [114] |
| ZnO | $Zn(NO_3)_2 \bullet 6H_2O$, NaOH (10 M[a]) | $H_2O$ + ethanol + ethylenediamine | 46 nm in diameter, 1.54 54 μm mu;m in length | Nanorod | [89] |
| $HfO_2$ | Hf metal chips | $H_2O$ | 25–35 nm | Monoclinic nanoparticle | [115] |
| $ZrO_2$ | $ZrCl_4$, $NH_4OH$, KF/NaOH/LiCl/KBr | $H_2O$ | 15–20 nm | Tetragonal and monoclinic nanoparticle | [116] |
| α-$Fe_2O_3$ | $Fe(NO_3)_3 \bullet 9H_2O$, Poly(N-vinyl-2pyrrolidone) | N, N-dimethylformamide | 30–50 nm | Quasicubic nanoparticle | [117] |
| CuO | Copper acetate | Ethanol | 3–9 nm | Nanoparticle | [118] |
| $Al_2O_3$ | $Al(NO_3)_3 \bullet 9H_2O$, $NH_4OH$, camphorsulfonic acid | $H_2O$ | ~28 nm in diameter, ~460 nm in length | Nanotube | [119] |

[a]Concentration of KOH or NaOH used in the solution

**Table 5** Typical ternary metal oxides achieved via hydrothermal/solvothermal process

| Compound | Starting materials | Solvent | Particles size | Morphology | References |
|---|---|---|---|---|---|
| $BaTiO_3$ | $Ti[OH(CH_3)_2]_4$, $Ba(OH)_2 \bullet 8H_2O$ | Ethanol + 2-methoxyethanol + acetic acid | 5–37 nm | Nanoparticle | [120] |
| $K_2Ti_6O_{13}$ | $TiO_2$ powder, KOH (10 M) | $H_2O$ | 10 nm in diameter, 500 nm–2 2 μm mu;m in length | Nanowire | [121] |
| $KNbO_3$ | $Nb_2O_5$ powder, KOH | $H_2O$ | 60 nm in diameter, 6 6 μm mu;m in length | Nanowire | [122] |
| $NaTaO_3$ | $Ta_2O_5$ powder, NaOH | $H_2O$ | 200 nm | Cubic nanoparticle | [123] |
| NaNbO3 | $Nb_2O_5$, NaOH | $H_2O$ | 100 nm–3 μm | Polyhedron particle | [123] |
| $ZnGa_2O_4$ | $GaCl_3$, HCl, Zn metal powder | $H_2O$ | 10 nm | Spherical nanoparticle | [124] |
| $BaZrO_3$ | Ba metal, zirconium isopropoxide isopropanol | Benzyl alcohol | 2–3 nm | Nanoparticle | [125] |
| LiNbO3 | Li metal, niobium ethoxide | Benzyl alcohol | 20–50 nm | Nanoparticle | [125] |

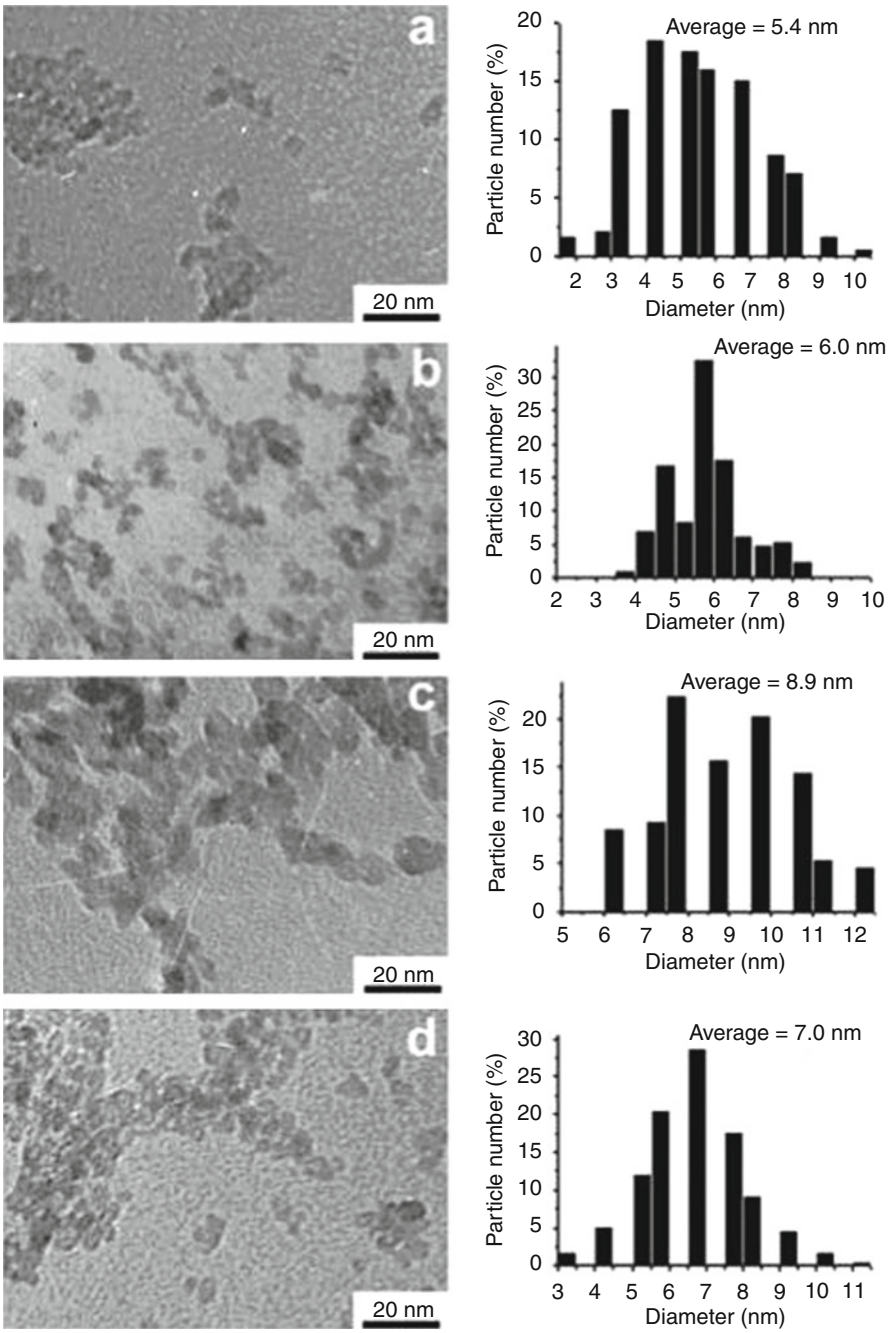


**Fig. 4** (continued)

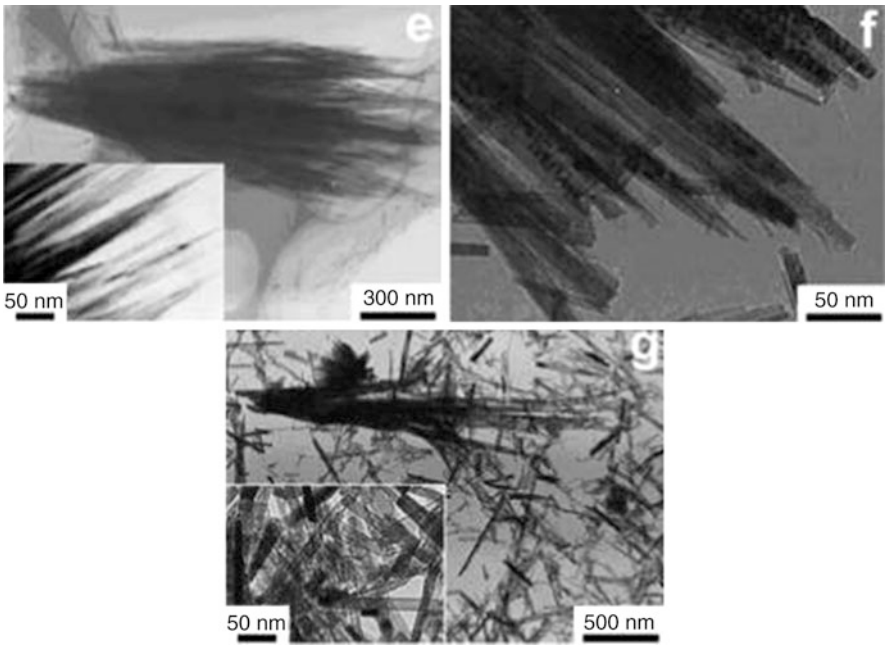


**Fig. 4** Transmission electron microscope (TEM) images of $TiO_2$ obtained in the solvothermal process with various $TiCl_4$/acetone (AC) ratios and operating temperatures. The $TiCl_4$/AC used was 1/90 (**a**), 1/30 (**b**, **d**), 1/15 (**c**), 1/10 (**e**, **g**), and 1/7 (**f**). The operating temperature used is 110 °C (**a**, **b**, **c**, **e**, **f**), and 140 °C (**d**, **g**). The graphs in the column on the right indicate the particle size distribution obtained from the TEM images shown on the left (Reproduced with permission from Wu et al. [133]. Copyright 2007, American Chemical Society)

solvents is also beneficial if the intent is to dope anions into the titania phase [134, 135].

Additives that act as structure-directing agents during the crystal growth are also crucial factors in the hydro-/solvothermal process. For instance, anatase $TiO_2$ NPs can be transformed from an irregular spherical shape to a rod-like shape in a solvothermal process if acetic acid is introduced to the solution. The anisotropic growth of the titania crystal was attributed to the attachment of acetic acid to the crystal plane [136]. Depending on the precursors and solvents used, the additives could change the phase and morphology of final titania products. For instance, in the ethanol/$TiCl_4$ solvothermal system, rutile nanofibers or nanorods were observed with $f = 1$, where $f$ *is* defined as the volume ratio between ethanol and acetic acid. A mixed anatase-rutile phase was obtained when $0.33 < f < 10$, and pure anatase NPs were produced in the rest of the $f$ region [137]. The morphology evolved from the submicrometer aggregates to microspheres and eventually to submicrometer aggregates by decreasing the $f$ [137].

Some additives can also function as a solvent, especially in a multiple-solvent system. For instance, anatase nanotubes, nanosheets, nanorods, and nanowires

could be obtained in a solvothermal solution containing aqueous NaOH ethanol [138], aqueous NaOH-ethylene glycol, or polyethylene glycol [139, 140]. This makes it difficult to distinguish additives from solvents and to further identify the role of additives, solvents, and mineralizers and thus leads to an ambiguous crystal growth mechanism.

## Group II–VI Nanoparticles

Group II–VI semiconducting nanomaterials have potential applications in the optoelectronic and energy industries. These nanomaterials include ZnS, ZnSe, ZnTe, CdS, CdSe, CdTe, HgS, HgSe, and HgTe as well as their doped and ternary compounds. Nanospheres of ZnS composed of 4 nm hexagonal NCs can be solvothermally synthesized in ethylene glycol using a single precursor, Zn $(NCS)_2(C_5H_5N)_2$, and an 80 % filling factor [141]. The nanospheres grow larger with increasing reaction temperature, reaching a size of 200, 350, and 450 nm in a 12 h reaction period at 160 °C, 180 °C, and 200 °C, respectively. Polycrystalline Mn-doped ZnS nanospheres can be synthesized in oleic acid using $ZnCl_2$, $MnCl_2$, and sulfur powders as the precursors at 180 °C for 60 h. These large (100 nm) nanospheres are actually aggregates of many tiny (10 nm) crystalline ZnS NPs [142]. Besides spheres (0-D), nanoplatelets (2-D) and nanorods (1-D) of ZnS can also be prepared hydrothermally or solvothermally [143, 144].

Cubic ZnSe and ZnTe NPs (NPs) can be synthesized via a solvothermal method that uses precursors that are less toxic than those used in the traditional chemical vapor deposition method [143]. The sources for Zn can be $Zn(CH_3COO)_2$, $ZnSO_4$, or Zn powders, and the precursors for Se and Te are elemental Se and Te powders or $Na_2SeO_3$ and $Na_2TeO_3$. Common solvents for the synthesis include ethylenediamine, ammonia, triethylamine, and hydrazine, and the pH usually maintains at 9–10. For example, crystalline ZnSe NCs can be synthesized by heating Zn and Se powders in a 1:1 ratio in a 90 % filled Teflon-lined autoclave at 120 °C for 6 h [145]. These nanomaterials consist of a mixture of NPs, short nanorods, and nanocubes with broad size distributions. ZnSe nanorods with more controllable morphology can be obtained by solvothermal reaction of $ZnSO_4$ and Se in triethylamine with the presence of the reducing agent $KBH_4$. The width of the nanorods is mostly between 30 and 70 nm [146]. ZnSe nanorods can be synthesized by heating Zn and Te powders in a 1.1:1 ratio in a 70 % filled Teflon-lined autoclave at 170 °C for 16 h. The nanorods are very uniform with a typical width of ~50 nm [147].

Highly uniform CdS spheres can be obtained using an ethylene glycol solvothermal method. $Cd(NO_3)_2$ and thiourea are used as precursors, and polyvinylpyrrolidone (PVP) is employed as a capping agent [148]. A stainless steel autoclave lined with polytetrafluoroethylene (PTFE) is used as the reactor, and the filling factor is 70 %. The CdS NPs grow from 150 to 450 nm if the reaction time is increased from 5 to 75 min at 140 °C [148]. The NP size also increases with increasing $Cd^{2+}$ concentrations. For example, the particle size increases from

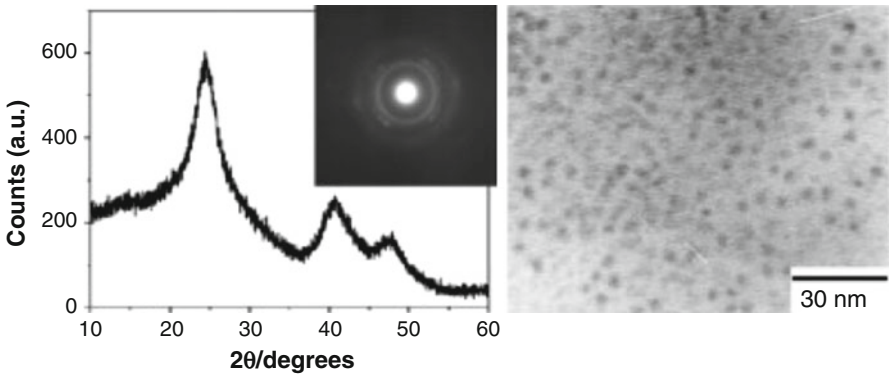


**Fig. 5** X-ray diffraction and selected-area electron diffraction (SAED) (*left*) and transmission electron microscope image (*right*) of the thioglycolic acid-stabilized CdTe nanocrystals (Reproduce with permission from Zhang et al. [145]. Copyright 2003, John Wiley and Sons)

100 to ~400 nm when the total concentration of $Cd^{2+}$ ions is increased from 0.02 to 0.2 M while maintaining the temperature, time, and concentration of capping agents at 140 $^{\circ C}$, 8 h, and 0.2 M, respectively [148]. In contrast, the NP size reduces with increasing PVP concentration, from 310 to 210 nm, when PVP increases from 0.05 to 0.5 M. These PVP molecules might function as nucleation sites during crystal growth. Higher PVP concentrations mean more available nucleation sites, which mitigate particle growth and result in smaller particles [148]. This method can also be applied to other sulfides, such as HgS, $Ag_2S$, and $Bi_2S_3$ [148]. Thioglycolic acid and dithiol glycol can also be used as S sources for the synthesis of CdS NPs via hydrothermal or solvothermal methods [149, 150].

Highly crystalline cubic zinc-blende CdTe has been obtained by the hydrothermal reaction of $CdCl_2$ and NaHTe in the presence of stabilizing agents such as thioglycolic acid, 3-mercaptopropionic acid, or 1-thioglycerol and at temperatures ranging between 100 °C and 180 °C (Fig. 5) [145, 147]. The rate of crystal growth is faster at higher temperature, as confirmed by both powder X-ray diffraction (XRD) and the red shift of the absorption spectra. Longer reaction time results in a larger crystal size and a larger red shift in their photoluminescence spectra due to the Ostwald ripening effect. In contrast, higher reactant concentration favors nucleation and produces smaller crystals.

Although mercury chalcogenides possess some unique properties and can be applied to sensors, photoelectronic devices, and transducers, but because the toxicity of mercury is high, research on these materials is very rare compared with the research on other II–VI compounds [151]. Traditional wet chemistry methods can also be utilized to grow II–VI NPs with well-controlled shapes and sizes [143, 151], but hydrothermal and solvothermal methods have the advantage of one-pot synthesis without the need of post-synthetic annealing to crystallize the NPs and thus provide greater potential for scale-up.

## Group III–V Nanoparticles

Group III–V nitrides, arsenides, and phosphides are very important direct band-gap semiconductors that have broad applications in optoelectronic devices such as light-emitting diodes, lasers, photodetectors, and optical amplifiers. The most important III–V compound is GaN, which has been commercially used in the LED bright-display panels.

The breakthrough in solvothermal synthesis of GaN was first reported by Xie et al. [152]. Polycrystalline GaN with a mixture of hexagonal and rock salt phases can be produced by a benzene solvothermal reaction of $GaCl_3$ and $Li_3N$ at 280 °C for 6–12 h in a silver-lined stainless steel autoclave with a filling factor of 75 %. The chemical reaction is shown in Eq. 6:

$$GaCl_3 + Li_3N \rightarrow GaN + 3LiCl \tag{3}$$

The LiCl salt is a by-product and can be removed by ethanol rinsing. The total yield is up to 80 %, and GaN shows an average diameter of 32 nm. However, no quantum effect is observed because the size is much larger than its Bohr exciton radius (11 nm). This novel benzene solvent method can be carried out at much lower temperature than that required in traditional methods. For example, hexagonal GaN is synthesized at around 900 °C by traditional gas-phase reaction between Ga metal and ammonia gas.

$GaCl_3$ and $NaN_3$ can also be used to synthesize GaN NPs in tetrahydrofuran (220 °C) or toluene (260 °C) via a solvothermal method [153]. It is a time-consuming reaction (2–4 days), and extreme caution should be exercised during the reaction because the metal azides are thermally unstable and shock sensitive. The product is a mixture of NPs and nanorods. The NPs have wide diameter distribution, from 20 nm to several hundred nanometers. The reaction mechanism is shown in Eqs. 4 and 5:

$$GaCl_3 + 3\,NaN_3 \rightarrow Ga(N_3)_3 + 3NaCl \tag{4}$$

$$Ga(N_3)_3 \rightarrow GaN + 4N_2 \tag{5}$$

GaN NPs having a diameter of several hundreds of nanometers can also be synthesized using anhydrous ammonia as a solvent (Table 5) [154]. The anhydrous ammonia is condensed into a quartz tube containing the reactants, and the tube is flame sealed. The pressure in the quartz tube is balanced with water held in an exterior pressure vessel at a pressure of about 10,000 psi. The temperature gradient along the tube is 10 °C/cm. Metal Ga, $GaI_2$, or $GaI_3$ can be used as Ga sources. Additives such as $NH_4I$, $NH_4Cl$, or $NH_4Br$ are required to generate GaN with Ga as the source. Temperature is critical in the synthesis of GaN when this ammoniathermal method is used. No GaN can be obtained below 250 °C. When the growth temperature is below 300 °C, only cubic phase and amorphous GaN NPs can be produced, and they are only deposited on the bottom of the tube reactor. In

contrast, above 440 °C, most products are composed of hexagonal GaN, and they are deposited on the middle wall of the tube. As-synthesized cubic GaN can be transformed to hexagonal GaN by annealing above 440 °C. $GaI_2$ or $GaI_3$ can also be used as the Ga source. The detailed experimental conditions are listed in Table 6. $GaI_2$ will disproportionate into Ga and $GaI_3$ immediately in ammonia.

Gallium imide-iodide (Ga-NH-I) can be prepared by reaction of $GI_3$ with $KNH_2$ in ammonia. When it is used as a precursor, only cubic GaN NCs can be obtained. However, this experiment is highly non-reproducible, probably due to an uncontrollable introduction of impurities like Si grease or poly(dimethylsiloxane) in the imide synthesis reaction [154].

GaN NPs with a very narrow size distribution (the average diameter is ~4 nm) can be synthesized via a toluene solvothermal method at 240 °C if Ga cupferron [$Ga(C_6H_5N_2O_2)_3$] (a metal-organic complex) is used as the Ga source and hexamethyldisilazane (HMDS) [$(CH_3)_3SiNHSi(CH_3)_3$] is used as the nitriding reagent [155] with a filling factor of 30 %. The diameter increases from 4 to 12 nm with decreasing Ga cupferron/HMDS by five times. It is believed that the Ga cupferron is first decomposed into $Ga_2O_3$ NPs, which then react with the HMDS at high temperature to form GaN NPs as shown in the following equation (Eq. 6):.

$$GaO_{1.5} + (CH_3)_3SiNHSi(CH_3)_3 \rightarrow GaN + (CH_3)_3SiOSi(CH_3)_3 + 1/2\,H_2O \quad (6)$$

With the presence of the capping reagent cetyltrimethylammonium bromide (CTAB), the diameter can be further reduced to 2.5 nm with a narrower size distribution (from 1 to 5 nm). If the Ga cupferron is replaced with $GaCl_3$ as shown in Eq. 7, the Ga NPs become larger with a wider size distribution (from 5 to 15 nm):

$$GaCl_3 + (CH_3)_3SiNHSi(CH_3)_3 \rightarrow GaN + 2Si(CH_3)_3Cl + HCl \quad (7)$$

Metal-ion-doped GaN NPs can be synthesized using a similar method with slightly different precursors. For example, ferromagnetic Mn-doped GaN with potential applications in spintronics can be synthesized by using $(Ga_{1-x}Mn_x)(C_6H_5N_2O_2)_{3(1-x)+2x}$ as the precursor [156]. 3 % Mn-doped GaN NCs can be obtained by the reaction of $(Ga_{0.97}Mn_{0.3})(C_6H_5N_2O_2)_{2.97}$ with HMDS in toluene in a 30 % filled Swagelok autoclave at 350 °C for 20 h. Average diameter of as-synthesized NPs is about 4 nm with a size distribution between 2 and 8 nm. Apparently, the introduction of dopants can significantly affect the crystallinity of the NPs, and post-synthetic annealing is required to obtain crystalline NPs as confirmed by powder XRD. However, the size increases to 18 nm after being annealed at 500 °C in $NH_3$ gas for 3 days. It seems that the amount of Mn doping does not affect the size of the NPs because 3 % and 5 % Mn-doped GaN NPs have the same size (4 nm) under the same synthetic conditions. The size of NPs increases to 6 nm when $GaCl_3$, $MnCl_2$, and HMDS are used as the reactants. The same method can also be used to synthesize 10 nm 5 %–10 % in-doped GaN NPs with $(Ga_{1-x}In_x)(C_6H_5N_2O_2)_3$ as the precursor [157].

**Table 6** Experimental data for the solvothermal synthesis of GaN nanocrystals from Ga metal and Ga iodides precursors [154]

| Exp | Reactants (mg) | mmol $NH_3$ | Fill (%)[a] | Temp pgm., °C[b] (16.67 h unless noted) | Products: appearance, X-ray analysis, and yield | | | |
|---|---|---|---|---|---|---|---|---|
| | | | | | bottom of tube[c] | yld (mg)[d] | Middle of tube[c] | yld (mg)[a] |
| **(I) No acid, or a small amount of $NH_4I$** | | | | | | | | |
| 1 | Ga (20) | 19.2 | 58 | 495 | | No reaction | | |
| 2 | Ga (33), $NH_4I$ (2.5) | 19.7 | 61 | 413 | ow pdr, 95 % h-GaN | 24 | Nothing | |
| 3 | Ga (18), $NH_4I$ (3.5) | 20.1 | 59 | 506 | gr pdr, 85%h-GaN | 9 | yl dep, 90 % c-GaN | 4 |
| **(II) ~0.5 M equiv of $NH_4I$, temperature varied** | | | | | | | | |
| 4 | Ga (22), $NH_4I$ (23) | – | 66 | 204 | | No reaction | | |
| | Above tube | | | Reheat 261 | yl pdr + Ga metal | – | Nothing | |
| | Above tube | | | Reheat 298 | tan pdr, 95%c-GaN[e] | – | Nothing | |
| 5 | Ga (27), $NH_4I$ (26) | 19.7 | 64 | 318 | tan-wh pdr, 55 % c-GaN + Ga metal | | Nothing | |
| 6 | Ga (26), $NH_4I$ (26) | 19.7 | 64 | 349 | ow pdr, 65 % h-GaN | 22 | Nothing | |
| 7 | Ga (31), $NH_4I$ (32) | 19.2 | 60 | 383 | ow pdr, 55 % h-GaN | – | Nothing | |
| 8 | Ga (31), $NH_4I$ (30) | 19.2 | 57 | 406 | ow pdr, 50 % h-GaN | – | Nothing | |
| 9 | Ga (29), $NH_4I$ (29) | 19.2 | 62 | 425 | ow pdr, 65 % h-GaN | 29 | Nothing | |
| 10 | Ga (31), $NH_4I$ (31) | 19.7 | 65 | 430 | ow pdr, 75 % h-GaN | 19 | Nothing | |
| 11 | Ga (28), $NH_4I$ (28) | 19.2 | 63 | 446 | ow pdr, 75 % h-GaN | 17 | yl dep, 100 % c-GaN | 3 |
| 12 | Ga (27), $NH_4I$ (28) | 19.2 | 64 | 448 | ow pdr, 80 % h-GaN | 21 | yl cls, 100 % c-GaN | 1.0 |
| 13 | Ga (22), $NH_4I$ (16) | – | 61 | 470 | Nothing | | or dep, 80 % c-GaN | 21 |
| 14 | Ga (20), $NH_4I$ (20) | 19.2 | 60 | 497 | Nothing | | or dep, 100 % c-GaN | 19 |
| **(III) 1 M equiv of $NH_4I$** | | | | | | | | |
| 15 | Ga (30), $NH_4I$ (60) | 19.7 | 64 | 453 | ow pdr, 100 % h-GaN | 14 | yl-or cls, 75 % c-GaN | 0.9 |
| 16 | Ga (70), $NH_4I$ (140) | – | 64 | 514 | | gr cls, h-GaN[f] | | |

| | | | | | | | | |
|---|---|---|---|---|---|---|---|---|
| **(IV) 0.5 M equiv of $NH_4I$, fill varied** | | | | | | | | |
| 17 | Ga (25), $NH_4I$ (25) | 12.8 | 42 | 459 | ow pdr 85 % h-GaN | 3 | or dep, >95 % c-GaN | 6.5 |
| 18 | Ga (28), $NH_4I$ (28) | 22.4 | 72 | 461 | ow pdr, 100 % h-GaN | 13 | or cls, c-GaN | 0.1 |
| **(V) Multistep temperature programs** | | | | | | | | |
| 19 | Ga (42), $NH_4I$ (38) | 19.7 | 59 | 305 (48 h); 25; 410 | ow pdr, 80 % h-GaN | 31 | Nothing | |
| 20 | Ga (31), $NH_4I$ (30) | 19.2 | 59 | 306 (40 h); 25; 455 | – | | gr dep, 95 % h-GaN | 21 |
| 21 | Ga (19), $NH_4I$ (18) | 18.3 | 62 | 350; 455 | ow pdr, 50 % c-GaN | 8 | or cls, 100 % c-GaN | 5 |
| 22 | Ga (37), $NH_4I$ (39) | 19.2 | 60 | 360; 510 | Nothing | | yl + wh cls,85 % h-GaN | 40 |
| 23 | Ga (28), $NH_4I$ (28) | 19.7 | 58 | 405; 455 | ow pdr + or cls, 65 % h-GaN[g] | 10 | or + gr cls, 95 % c-GaN | 10 |
| **(VI) $NH_4Cl$ or $NH_4Br$ mineralizer** | | | | | | | | |
| 24 | Ga (25), $NH_4Cl$ (9) | 19.8 | 63 | 453 | ow pdr, 100 % h-GaN | >8 | gn dep, 100 % c-GaN | 3.5 |
| 25 | Ga (40), $NH_4Cl$ (13) | 13.0 | 41 | 454 | ow pdr, 100 % h-GaN | 5 | ow dep, 60 % h-GaN | 0.2 |
| 26 | Ga (20), $NH_4Br$ (20) | 20.1 | 64 | 455 | ow pdr, 65 % h-GaN | 3 | yl + gr cls, 80 % c-GaN | 12 |
| 27 | Ga (28), $NH_4Br$ (19) | 19.7 | 66 | 466 | ow pdr, 60 % h-GaN | 2 | yl + gr cls, 70 % h-GaN | 15 |
| **(VII) $GaI_2$ or $GaI_3$ precursor** | | | | | | | | |
| 28 | $GaI_2$ (100) | 19.4 | ~60 | 435 (64 h) | ow pdr, 80 % h-GaN | 4 | ub- or dep 90 % c-GaN | 13 |
| | | | | | | | lb- gr dep 60 % h-GaN | 15 |
| 29 | $GaI_2$ (100) | 19.5 | 62 | 350; 25; 455 | ow pdr, 80 % h-GaN | 10 | gr dep, 100 % h-GaN | 14 |
| 30 | $GaI_3$ (80) | 19.2 | 61 | 416 | or pdr, 100 % c-GaN | 6 | Nothing | |

(*continued*)

**Table 6** (continued)

| Exp | Reactants (mg) | mmol $NH_3$ | Fill (%)[a] | Temp pgm., °C[b] (16.67 h unless noted) | Products: appearance, X-ray analysis, and yield | | | |
|---|---|---|---|---|---|---|---|---|
| | | | | | bottom of tube[c] | yld (mg)[d] | Middle of tube[c] | yld (mg)[a] |
| 31 | $GaI_3$ (100) | 19.2 | 64 | 419 | or-tan pdr, 80%c-GaN | 11 | Nothing | |
| 32 | $GaI_3$ (273) | 19.2 | – | 466 | gr pdr, 60 % h-GaN | 17 | or dep, >95 % c-GaN | 6 |
| 33 | $GaI_3$ (200) | 20.1 | 66 | 491 | Nothing | | or dep, 100 % c-GaN | 12 |

*pdr* powder, *dep*. deposit, *cls* clusters of crystals, – datum not available, *or* orange, *yl* yellow, *gr* gray, *gn* green, *wh* white, *ow* off-white, *ub* upper band, *lb* lower band

[a]Fraction of volume filled with solid and liquid at room temperature

[b]Actual temperatures measured in thermowell at least 3 h after heating begins (typically ~50 °C below furnace setting). The furnace on time at each temperature is 16.67 h unless noted otherwise

[c]Percentages are indicate the fraction of crystalline GaN in the cub and hex form: only

[d]Isolated yield. Not measured for all experiments

[e]May contain an amorphous product

[f]Tube burst from excess $H_2$ pressure when exterior counterpressure was relieved

[g]C–GaN clusters may have fallen from above

Other metal nitrides, such as NbN, ZrN, HfN, and $Ta_3N_5$, can also be prepared through a similar strategy. Using $TaCl_5$, $ZrCl_4$, $HfCl_4$, and $NbCl_5$ as the metal precursor and $LiNH_2$ as the nitriding reagent, crystalline NPs of $Ta_3N_5$, ZrN, HfN, and NbN of variable sizes can be prepared through a benzene solvothermal reaction at 550 °C for 24 h [158]. However, only amorphous NPs are observed below 450 °C. The methods for the synthesis of other nitrides, phosphides, and arsenides are similar to the abovementioned ones (see Table 7).

## Group IV Nanoparticles

The most important Group IV NPs include those containing carbon, silicon, and germanium. Carbon-based NPs include carbonaceous and composite carbonaceous NPs (i.e., carbon modified with magnetic, optical, catalytic, or other materials).

Carbonaceous and composite carbonaceous nanomaterials have broad applications in environmental remediation, catalysis, bioimaging, and drug delivery and in the manufacture of lithium ion batteries, fuel cells, and sensors [164]. The focus is on low temperature hydrothermal methods used to synthesize carbonaceous NPs (high-temperature hydrothermal methods, which can be used to synthesize advanced carbon structures such as carbon nanotubes, activated carbon, carbon thin films, and graphite, but they are not the focus of this chapter.).

The hydrothermal precursors for carbon NPs can be sugar, glucose, cyclodextrins, fructose, sucrose, cellulose, and starch, all of which are biocompatible and relatively cheap [165]. The morphology of carbon NPs tends to be spherical. Reaction temperature is critical in formation of carbon spheres. No carbon spheres are obtained below 140 °C. In contrast, with 0.5 M glucose as the C source and a 160 °C reaction temperature, carbon spheres of 200, 500, 800, 1,100, and 1,500 nm in diameter can be produced after a reaction time of 2, 4, 6, 8, and 10 h, respectively. The growth of these NPs consists of dehydration, condensation, polymerization, and aromatization processes. The presence of metal ions and metal oxides such as $Fe^{3+}$ and $Fe_2O_3$ can significantly catalyze the process of carbonization of carbon precursors. The reaction temperatures usually range from 150 °C to 350 °C, and the reaction time is between 4 and 24 h. Depending on the precursors, the sizes of the NPs vary from 100 nm to several micrometers.

Porous carbon NPs can be prepared on mesoporous or nonporous silica templates. After the NPs are deposited on the templates, the templates are selectively etched away (Fig. 6). Surface wettability plays an extremely important role. If the surface of the templates cannot be wetted by the precursor, no porous carbon NPs can be obtained [166, 167]. In addition, when the triblock copolymer Pluronic F127 is used as a template and phenolic resol is used as a carbon source, more-uniform mesoporous carbon NPs can be produced. The reaction can be tuned by varying the reagent concentration to produce NPs whose sizes range from 20 to 140 nm. For example, carbon NPs of 140 nm and 20 nm can be synthesized through a hydrothermal reaction at 130 °C in a solution of phenol and water in ratios of 1:200 and 1:450, respectively [168]. Although this method is elegant, the cost is too high for

**Table 7** Synthesis of other III–V nanomaterials using hydrothermal and solvothermal methods

| Compound | Size of NPs (nm) | Morphology | Solvent | Surfactant | Temperature (°C) | Time (h) | Precursors |
|---|---|---|---|---|---|---|---|
| BN [159] | 150 | Hollow hexagon sphere | $BBr_3$ | N/A | 400–450 | 6–12 | $BBr_3$, $NH_4Cl$, and $NaNH_2$ |
| InP [160] | 8 | Sphere | Ammonia | Potassium stearate | 140 | 8–12 | $InCl_3$, $NBH_4$, and elemental P |
| InAs [161] | 12 | Sphere | Xylene | N/A | 150 | 48 | $InCl_3$, $AsCl_3$, Zn |
| GaP [162] | 2–48 | Sphere | Benzene | N/A | 300 | 0–24 | $Na_3P$, $GaCl_3$ |
| GaAs [163] | 20–50 | Sphere | $H_2O$ | N/A | 180–190 | 24 | $As_2O_3$, metal Ga, $H_2SO_4$ |

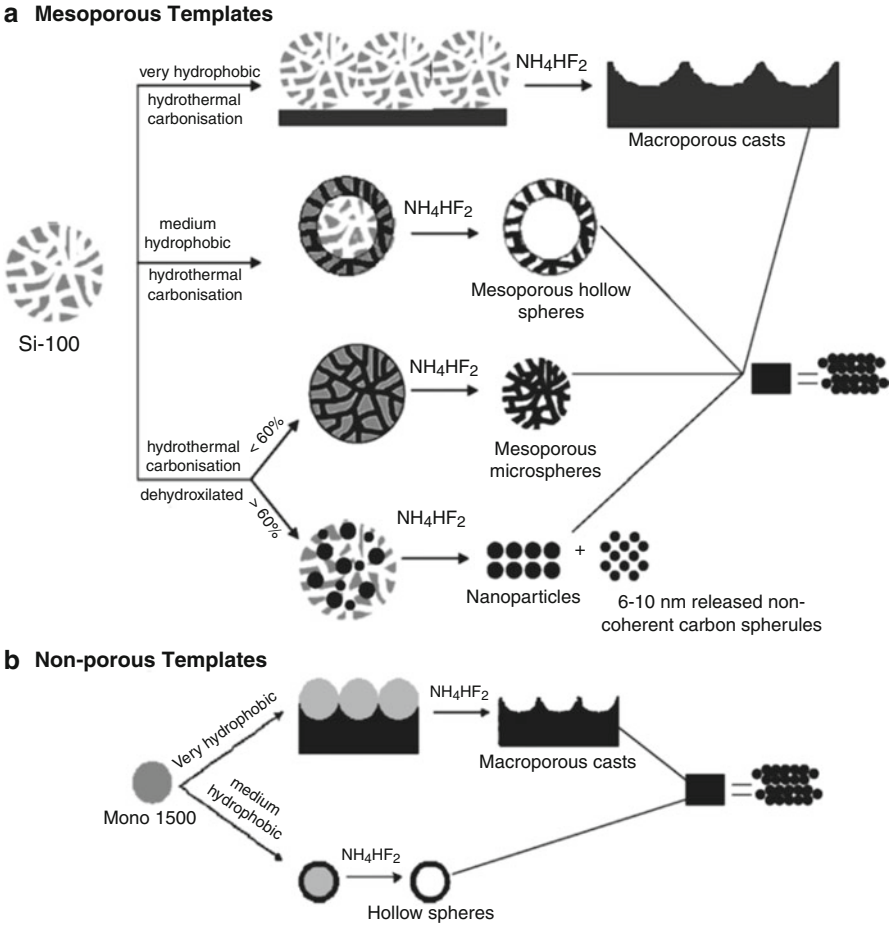


**Fig. 6** Schematic representation of the hydrothermal carbonization process using silica templates with different polarities, resulting in the formation of various carbon morphologies (Reproduced with permission from Titirici et al. [166]. Copyright 2007, John Wiley and Sons)

practical large-scale applications. Similarly, this one-pot hydrothermal method can be extended to the synthesis of composite carbonaceous NPs by simply mixing the metal precursors or metal oxide NPs (e.g., Ag, Pd, Se, $Fe_3O_4$, $SnO_2$) with a carbon source [167]. Alternatively, such composite materials can be prepared via a post-synthetic treatment of as-synthesized hydrothermal carbonaceous NPs.

Silicon and germanium are highly important semiconductors due to their broad applications in the electronic and optoelectronic industries. Solvothermal and hydrothermal methods to grow Si and Ge NPs are extremely challenging and often require very high temperature to initiate crystallization. Ge NPs with poor crystallinity can be synthesized by decomposition of tetraethylgermanium in organic solvents or superfluidic solvents such as $CO_2$ with and without surfactants

at high temperature. The surfactants have three functions: (1) forming inverse micelles to guide nucleation and crystal growth (size control), (2) morphology control of the Ge NPs (shape control) by selective adsorption on certain crystal planes, and (3) stabilizing nanoscale particles (stability control) by reducing the surface energy of NPs through surface adsorption on those NPs. Ge nanocubes of 100 nm edge length can be synthesized using a hexane solvothermal method with a surfactant additive, heptaethylene glycol monododecyl ether ($C_{12}E_7$) [169]. Equimolar amount of $GeCl_4$ and phenyl-$GeCl_3$ is used as the Ge precursors, and metallic Na dispersed in toluene is employed as the reducing reagent. The mixture is heated at 280 °C for 3 days in a Parr 4750 reactor without stirring or shaking. The filling factor is about 65 %. NaCl, a by-product, can be removed by vigorous rinsing with ethanol, water, and hexane. The as-synthesized Ge nanocubes are highly crystalline with a diamond cubic structure (a = 5.655 Å), as confirmed by both powder XRD and high-resolution TEM. These 100 nm nanocubes are composed of multiple smaller nanocubes, which are connected to each other through the surface-adsorbed surfactant molecules. When the surfactant is changed to pentaethylene glycol ether (C12E5), a mixture of spherical, triangular, and hexagonal Ge NPs is produced with diameters ranging from 15 to 70 nm (Fig. 7) [170]. The shape of Ge NPs can be tuned by controlling surfactant amount. For example, only Ge spheres with diameters between 6 and 35 nm are yielded if the amount of surfactant is reduced by three times (1.8 ml to 0.6 ml). The yield of Ge NPs is mainly affected by the reaction time. Extending the reaction time from 4 to 12 h enhances the yield from 35 % to 54 %. However, the size and crystallinity of these NPs are independent of the reaction time, probably due to the presence of the capping surfactant molecules. Other Group IV NPs, such as Si, can also be synthesized using such a solvothermal method [171].

## Transition Metal Nanoparticles

Metallic NPs possess many unique optical, electronic, and magnetic properties that can be applied to catalysts, sensors, and memory devices. Although wet chemistry methods (with reducing agents and capping surfactants) can be used for controllable synthesis of metal NPs, hydrothermal and solvothermal methods provide better control of morphology and crystallinity. Usually, the NPs are deposited or loaded onto a support material to increase their reactivity and recyclability.

Extremely small (1.7 nm) Pt particles have been synthesized using an ethylene glycol solvothermal method at basic conditions [172]. The ethylene glycol functions both as the solvent and as a reducing agent; $H_2PtCl_6.6H_2O$ serves as the Pt precursor. The mixture was heated to 433 K for 3 h [172].

The ethylene glycol solvothermal method can also be utilized to grow Ag NPs [173]. In a typical procedure, $AgNO_3$ is added into a double-walled digestion vessel that has an inner Teflon liner and an outer high-strength shell. Then, appropriate amounts of toluene, ethylene glycol, and dodecylthiol (thiol) are added into the

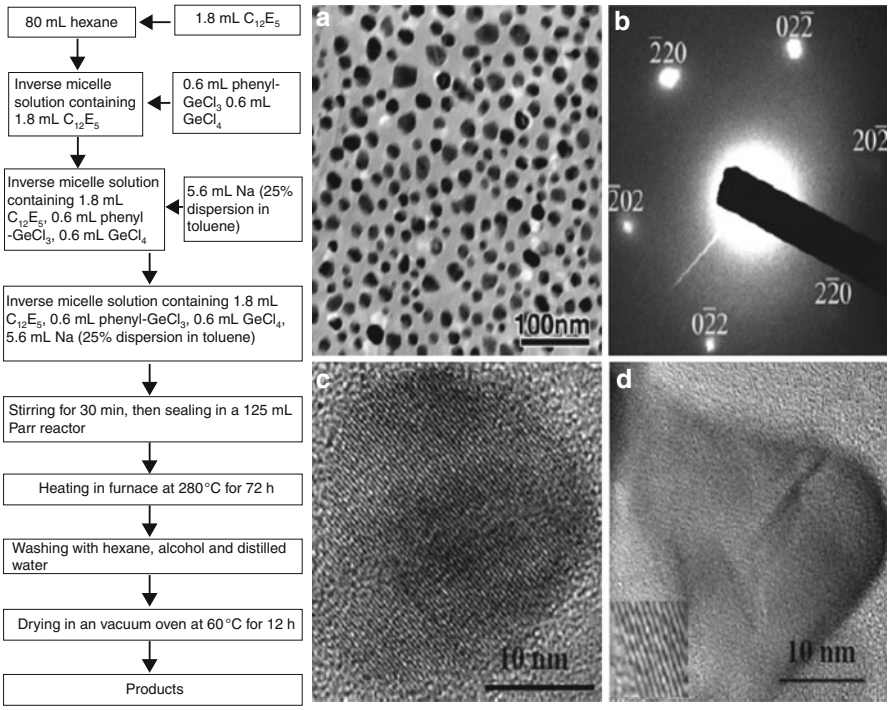


**Fig. 7** Diagram showing the fabrication method to obtain Ge nanocubes (*left*); *Right*: (**a**) transmission electron microscope (TEM) images of the Ge nanocrystals; (**b**) selected-area electron diffraction pattern of Ge nanocrystals; (**c**) high-resolution TEM image of spherical and (**d**) triangular Ge nanocrystals. (Reproduced with permission from Wang et al. [170]. Copyright 2005, Institute of Physics)

vessel in that order. The solvothermal reaction is carried out at 160 °C to 170 °C for 3 h in a microwave digestion system. The Ag NPs have a very regular spherical shape and an average diameter of ~10 nm. The thiol functions as a complexing reagent, and the ethylene glycol is a mild reducing agent. Decreasing the ethylene glycol/thiol ratio from 3 to 1.5 can dramatically change the morphology of the Ag NPs from spherical to rectangular with a slightly reduced diameter (6–10 nm).

Pt NPs can also be synthesized using a dimethylformamide (DMF) solvothermal method in a sealed PTFE-lined reactor vessel [174]. The metal precursor is platinum (II), 2,4-pentanedionate ($Pt(acac)_2$), and DMF works as a mild reducing agent and solvent. The reaction mixture is heated in a furnace to 200 °C for 24 h. The same DMF solvothermal method can also be employed to grow Ag and Au NPs. Besides ethylene glycol and DMF, other reducing agents (e.g., $NaBH_4$, $N_2H_4$, $NH_2OH$, and ethanol) can also be used to grow transition metal NPs.

**Table 8** Metal content and Rietveld analysis of $Pt_xNi_{1-x}$ alloy nanoparticles, reproduced with permission from [174]. Copyright 2012, American Chemical Society

| | Analyzed metal content | | | XRD-derived values | | | | |
|---|---|---|---|---|---|---|---|---|
| Reactant Pt/Ni molar ratio | wt % Pt | wt % Ni | Pt/Ni molar ratio | Lattice parameter (Å) | Ni mole fraction | Pt mole fraction | Phase wt % | Average crystallite size (nm) |
| 0.5 | 23 | 11.8 | 0.6 | 3.7939 | 0.33 | 0.77 | 37 | 3.8 |
| | | | | 3.7368 | 0.47 | 0.53 | 63 | 6.1 |
| 1 | 25 | 8.5 | 0.9 | 3.8292 | 0.24 | 0.76 | 40 | 6.7 |
| | | | | 3.7529 | 0.43 | 0.57 | 60 | 6.7 |
| 1.5 | 27 | 4.8 | 1.7 | 3.8556 | 0.17 | 0.83 | 32 | 4.0 |
| | | | | 3.7840 | 0.35 | 0.65 | 68 | 7.4 |
| 2 | 27 | 3.8 | 2.1 | 3.8636 | 0.15 | 0.85 | 61 | 3.1 |
| | | | | 3.7976 | 0.32 | 0.68 | 39 | 5.9 |
| 3 | 29 | 2.7 | 3.2 | 3.8427 | 0.20 | 0.80 | 100 | 5.5 |

Bimetallic-alloy NPs can also be synthesized using the aforementioned method (Table 8) [174]. The only difference is that two metal precursors are added simultaneously. For instance, the DMF solvothermal method can be used to generate platinum-nickel alloy NCs. The metal precursors for Pt and Ni are platinum (II) 2,4-pentanedionate and nickel (II) 2,4-pentanedionate, respectively. In a typical reaction, the Pt and Ni acetylacetonates are dissolved in DMF to yield concentrations of 30 mM $Pt(acac)_2$ and 10 mM $Ni(acac)_2$. The reaction mixture is heated in a furnace to 200 °C for 24 h. The reaction is incomplete below 200 °C due to the slow decomposition of $Ni(acac)_2$ at that temperature. As-synthesized $Pt_3Ni$ NPs are highly crystalline and have diameters ranging from 11 to 13 nm. Variations in the ratio of the two precursors result in the synthesis of PtNi bimetallic-alloy NPs having various compositions and slight differences in diameter, as shown in Table 8. The same strategy can be used to prepare other bimetallic-alloy NPs (e.g., Pt-Co and Pt-Fe).

## Metal-Organic Framework Nanoparticles

In the past two decades, MOFs have attracted enormous research attention due to their potential applications for hydrogen storage [172], gas separation [173], catalysis [175], bioimaging [176], drug delivery [177, 178], sensors [179], and proton exchange membranes [180]. MOFs constitute a class of hybrid nanoporous crystalline materials consisting of metals and bridging organic linkers with pore sizes ranging from 0.4 to 6 nm [177]. MOFs are commonly synthesized through hydrothermal and solvothermal methods. Compared with the synthesis of Group II–VI and III–V NPs, the pressure and temperature used for MOF NP synthesis are much milder to avoid decomposition of organic ligands. Herein, only the synthetic methods for MOF NPs for biomedical applications are extensively discussed,

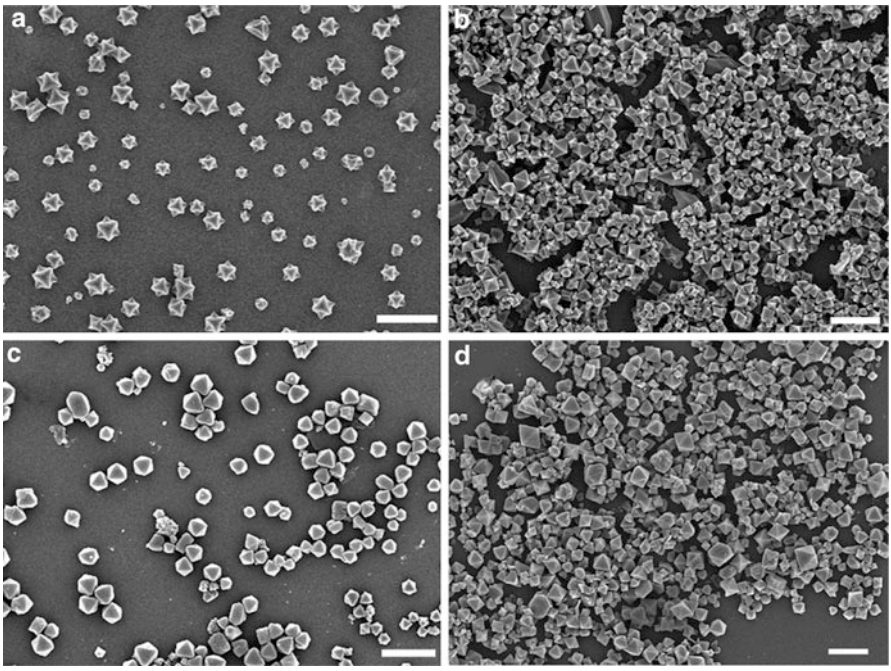


**Fig. 8** Scanning electron microscope (SEM) images of (**a**) $Fe_3(\mu_3\text{-}O)Cl(H_2O)_2(BDC)_3$ nanoparticles, (**b**) $Fe_3(\mu_3\text{-}O)Cl(H_2O)_2(BDC)_3$ nanoparticles incorporated with 17.4 mol % $NH_2$-BDC, (**c**) nanoparticles shown in image (**a**) loaded with 1,3,5,7-tetramethyl-4,4-difluoro-8-bromomethyl-4-bora-3*a*,4*a*-diaza-*s*-indacene dye molecules and (**d**) nanoparticles shown in image (**a**) loaded with *c*,*c*,*t*-$[PtCl_2(NH_3)_2(OEt)(O_2CCH_2CH_2CO_2H)]$ anticancer prodrug (Reproduced with permission from Taylor-Pashow et al. [181]. Copyright 2009, American Chemical Society)

mainly because such NPs are highly desirable. For other applications, thin film (gas separation) or bulk form (gas storage) shows superior performance:

(a) Crystal growth without a surfactant template

MOF NCs can be grown via a simple, straightforward solvothermal method. For instance, Fe(III) MOF NCs with a framework formula of $Fe_3\text{-}(\mu_3\text{-}O)Cl(H_2O)_2(BDC)_3$ (MIL 101; BDC = terephthalic acid) can be synthesized by simply microwave heating a solution of equal-molar $FeCl_3$ and BDC in DMF at 150 °C (Fig. 8) [181]. The microwave heating produces smaller particles with high reproducibility. The synthesized NPs are octahedral and have an average diameter of ~200 nm. The NPs are highly crystalline as confirmed by powder XRD, and the Langmuir surface area ranges from 3,700 to 4,535 $m^2/g$ [181]. The MOF NPs can be functionalized with dye molecules for cell imaging or anticancer prodrugs for cancer therapies. However, these functionalized $NP_S$ are chemically unstable in a physiological environment.

That limitation can be overcome by post-synthetic coating of the MOF NPs with a layer of silica [181].

(b) Crystal growth with surfactant template

Surfactant additives used in solvothermal and hydrothermal methods can form micelles, which functions as templates to guide the growth of NPs with controlled size, shape, and crystallinity. For example, highly paramagnetic Gd (III) MOF NPs can be synthesized via a surfactant-assisted hydrothermal method with or without microwave heating. To synthesize $[Gd_2(bhc)(H_2O)_6]$ MOF NPs (bhc = mellitic acid), CTAB/1-hexanol/n-heptane microemulsions are first added with an aqueous mellitic acid methylammonium salt and an aqueous $GdCl_3$ solution. Then they are loaded into a Teflon-lined Parr reactor and heated to 120 °C for 18 h to yield the NPs [182]. The MOF NPs have to be purified by repeated centrifugation at high speed and re-dispersion in an ethanol solution to completely remove surfactant impurities. As-synthesized MOF NPs are highly crystalline with a block shape (25 × 50 × 100 nm), and the yield is very high (84.4 %).

Hydrothermal growth is beneficial for obtaining highly crystalline NPs compared to the traditional wet chemistry growth. When the reaction is carried out at room temperature, only amorphous Gd MOF NPs can be obtained because the nucleation rate is too rapid and dominates the NP growth. Instead, using a 400 W microwave to heat the Teflon reactor to 60 °C produces final NPs that possess a nanorod shape with lengths up to several micrometers and widths ranging from 100 to 300 nm. The MOF NPs obtained under microwave heating have a formula of $[Gd_2(bhc)(H_2O)_8](H_2O)_2$ instead of $[Gd_2(bhc)(H_2O)_6]$. When the temperature is increased to 120 °C under 400 W microwave heating, the NPs are octahedral with larger diameters (1–2 μm). The synthesized Gd(III) MOFs can be applied to magnetic resonance imaging [182]. Similar hydrothermal methods can be employed to obtain Mn(II), Eu(III), and Tb(III) MOF nanomaterials [183, 184]. The microwave heating, reaction temperature, and water-to-surfactant ratio have significant impacts on the morphology of these synthesized MOF NPs. Lower temperature and a larger water-to-surfactant ratio lead to the growth of nanorods, whereas higher temperature and microwave heating result in shorter nanorods or octahedral NPs.

## Surface Treatment of Nanoparticles Using Hydrothermal and Solvothermal Methods and its Effect on Their Physicochemical Properties

Inorganic NPs have potential applications in various fields, including electronics, energy storage, catalysts, hybrid materials, and biomedical applications [185–188] due to their unique "quantum size effect" [189]. However, the practical application of inorganic NPs is hindered by the severe aggregation resulting from their high

surface area [190] and poor dispersion in organic solvents owing to the hydroxyl groups on their surfaces [191]. These issues could be addressed by modifying the surfaces of the NPs. Among the various methods that are available for modifying the surface of NPs, the hydrothermal and solvothermal processes are among the most promising techniques to improve the dispersibility and compatibility between inorganic NPs and organic solvents [192–195]. For instance, $-NH_2$ and –CHO groups can be successfully grafted onto the surface of AlOOH NPs through in situ surface modification via a hydrothermal process [188] that makes the hydrophilic surface of AlOOH NPs hydrophobic, resulting in modified AlOOH NPs that disperse well in solvents [188]. In the presence of caprylic acid and n-butylamine, $ZnO/TiO_2$ hybrid NPs show reduced agglomeration and enhanced dispersibility [192]. Successful surface modifications of other inorganic NPs via a hydrothermal process, including $Fe_3O_4$ [194] and $BaTiO_3$ [196], have also been reported.

## Conclusion

Hydrothermal and solvothermal techniques have been widely adopted as classic methods for the fabrication of inorganic and metal-organic nanomaterial, including oxides; Group III–V, II–IV, and VI elements; MOFs; and transitional metals. These techniques could be utilized to synthesize organic NPs, provided that the organic chemicals will not be decomposed at such high temperatures and pressures. However, methods to synthesize organic NPs are still under development and are limited by the stability of organic compounds. Additionally, organic NPs can be readily synthesized via a traditional wet chemistry method with or without the assistance of surfactants. Due to the unlimited combinations of metal ions and bridging organic ligands for MOF compounds, it would be worth exploring the MOF NP synthesis via hydrothermal and solvothermal methods. Such research could yield very interesting discoveries in the coming decades.

## References

1. K. Byrappa, M. Yoshimura, *Handbook of Hydrothermal Technology* (William Andrew, Norwich, 2001)
2. K.F.E. Schafthaul, Gelehrte Anzeigen Bayer. Akad. **20**, 557 (1845)
3. K. Byrappa, T. Adschiri, Progr. Cryst. Growth Character. Mater. **53**, 117 (2007)
4. Z.L. Wang, Adv. Mater. (Weinheim, Germany) **15**, 1497 (2003)
5. H.C. Helgeson, D.H. Kirkham, Am. J. Sci. **274**, 1089 (1974)
6. H.C. Helgeson, D.H. Kirkham, Am. J. Sci. **276**, 97 (1976)
7. H.C. Helgeson, D.H. Kirkham, G.C. Flowers, Am. J. Sci. **281**, 1249 (1981)
8. E.L. Shock, E.H. Oelkers, J.W. Johnson, D.A. Sverjensky, H.C. Helgeson, J. Chem. Soc. Faraday Trans. **88**, 803 (1992)
9. W. Dawson, J. Am. Ceramic Soc. Bull. **67**, 1673 (1988)
10. I. Sunagawa, K. Tsukamoto, K. Maiwa, K. Onuma, Progr. Crystal. Growth Character. Mater. **30**, 153 (1995)

11. B.E. Etschmann, W. Liu, D. Testemale, H. Mueller, N.A. Rae, O. Proux, J.L. Hazemann, J. Brugger, Geochim. Cosmochim. Acta **74**, 4723 (2010)
12. C. Gerardin, M. Haouas, C. Lorentz, F. Taulelle, Magn. Reson. Chem. **38**, 429 (2000)
13. S.R. Higgins, C.M. Eggleston, G. Jordan, K.G. Knauss, C.O. Boro, Mineral. Mag. **62A**, 618 (1998)
14. K. Kawamura, H. Nagayoshi, T. Yao, Anal. Chim. Acta **667**, 88 (2010)
15. J.E. Maslar, W.S. Hurst, W.J. Bowers Jr., J.H. Hendricks, Corrosion (Houston, TX, United States) **58**, 739 (2002)
16. J.E. Maslar, W.S. Hurst, W.J. Bowers, J.H. Hendricks, M.I. Aquino, I. Levin, Appl. Surf. Sci. **180**, 102 (2001)
17. P. Norby, Mater. Sci. Forum **228**, 147 (1996)
18. G.S. Pokrovski, J. Roux, J.L. Hazemann, A.Y. Borisova, A.A. Gonchar, M.P. Lemeshko, Mineral. Mag. **72**, 667 (2008)
19. K. Sue, M. Suzuki, K. Arai, T. Ohashi, H. Ura, K. Matsui, Y. Hakuta, H. Hayashi, M. Watanabe, T. Hiaki, Green Chem. **8**, 634 (2006)
20. T. Andelman, M.C. Tan, R.E. Riman, Mater. Res. Innov. **14**, 9 (2010)
21. T. Adschiri, Y. Hakuta, K. Arai, Ind. Eng. Chem. Res. **39**, 4901 (2000)
22. R.E. Riman, W.L. Suchanek, M.M. Lencka, Ann. Chim. (Paris, France) **27**, 15 (2002)
23. M.M. Lencka, R.E. Riman, J. Am. Ceram. Soc. **76**, 2649 (1993)
24. K.S. Pitzer, J. Phys. Chem. **77**, 268 (1973)
25. L.A. Bromley, AIChE J. **19**, 313 (1973)
26. J.F. Zemaitis Jr., D.M. Clark, M. Rafal, N.C. Scrivner, *Handbook of Aqueous Electrolyte Thermodynamics: Theory and Application*, 1st edn. (Wiley-AIChE, Hoboken, 1986)
27. K. Minami, T. Suzuki, T. Aizawa, K. Sue, K. Arai, R.L. Smith Jr., Fluid Phase Equilib. **257**, 177 (2007)
28. A.V. Plyasunov, E.L. Shock, Geochim. Cosmochim. Acta **65**, 3879 (2001)
29. D.A. Sverjensky, E.L. Shock, H.C. Helgeson, Geochim. Cosmochim. Acta **61**, 1359 (1997)
30. T. Adschiri, Y. Hakuta, K. Sue, K. Arai, J. Nanoparticle Res. **3**, 227 (2001)
31. D. Kashchiev, J. Chem. Phys. **76**, 5098 (1982)
32. B. Schoeman, J. Micro. Meso. Mater. **22**, 9 (1998)
33. C.E.A. Kirschhock, R. Ravishankar, P.A. Jacobs, J.A. Martens, J. Phys. Chem. B **103**, 11021 (1999)
34. V. Nikolakis, E. Kokkoli, M. Tirrell, M. Tsapatsis, D.G. Vlachos, Chem. Mater. **12**, 845 (2000)
35. M. Uematsu, E.U. Franck, J. Phys. Chem. Refer. Data **9**, 1291 (1981)
36. S. Yin, Y. Fujishiro, J. Wu, M. Aki, T. Sato, J. Mater. Process. Technol. **137**, 45 (2003)
37. M. Kang, J. Mol. Catal. A: Chem. **197**, 173 (2003)
38. C.-S. Kim, B.K. Moon, J.-H. Park, S.T. Chung, S.-M. Son, J. Crystal Growth **254**, 405 (2003)
39. Y. Zhu, T. Mei, Y. Wang, Y. Qian, J. Mater. Chem. **21**, 11457 (2011)
40. J. Li, Z. Chen, R.J. Wang, D.M. Proserpio, Coord. Chem. Rev. **192**, 707 (1999)
41. K. Han, S. Xia, P. Ma, F. Yan, T. Liu, J. Chem. Thermodyn. **62**, 111 (2013)
42. N.W. Krase, J.B. Goodman, Ind. Eng. Chem. **22**, 13 (1930)
43. A.S. Teja, D. Rosenthal, J. DIPPR Data Ser. **1**, 96 (1991)
44. S.-H. Yu, J. Ceramic Soc. Japan **109**, S65 (2001)
45. Y. Konishi, T. Kawamura, S. Asai, Ind. Eng. Chem. Res. **32**, 2888 (1993)
46. D. Chen, R. Xu, J. Mater. Chem. **8**, 965 (1998)
47. Z.-X. Deng, C. Wang, X.-M. Sun, Y.-D. Li, Inorg. Chem. **41**, 869 (2002)
48. J. Lu, P. Qi, Y. Peng, Z. Meng, Z. Yang, W. Yu, Y. Qian, Chem. Mater. **13**, 2169 (2001)
49. Y. Gao, M. Fan, Q. Fang, W. Han, New J. Chem. **37**, 670 (2013)
50. Z.-Y. Yuan, B.-L. Su, Colloid. Surf. A: Phys. Eng. Aspect. **241**, 173 (2004)
51. A. Nakahira, W. Kato, M. Tamai, T. Isshiki, K. Nishio, H. Aritani, J. Mater. Sci. **39**, 4239 (2004)
52. R. Lu, J. Yuan, H. Shi, B. Li, W. Wang, D. Wang, M. Cao, CrystEngComm **15**, 3984 (2013)

53. M. Safaei, R. Sarraf-Mamoory, M. Rashidzadeh, M. Manteghian, J. Porous Mater. **17**, 719 (2010)
54. G.W. Morey, P. Niggli, J. Am. Chem. Soc. **35**, 1086 (1913)
55. R. Nacken, Chemiker-Zeitung **74**, 745 (1950)
56. R.M. Barrer, Nature **157**, 734 (1946)
57. R.H. Ewell, H. Insley, J. Res. Nat. Bur. Stand. **15**, 173 (1935)
58. S.F. Adams, Econ. Geol. Bull. Soc. Econ. Geol. **15**, 623 (1920)
59. A.C. Walker, J. Am. Ceram. Soc. **36**, 250 (1953)
60. R.M. Barrer, C. Marcilly, J. Chem. Soc. [Section] A: Inorg. Phys. Theor. 2735 (1970)
61. P.B. Moore, Am. Mineral. **55**, 135 (1970)
62. H.C. Helgeson, Am. J. Sci. **267**, 729 (1969)
63. H.C. Helgeson, R.M. Garrels, F.T. Mackenzie, Geochim. Cosmochim. Acta **33**, 455 (1969)
64. F. Dachille, P.Y. Simons, R. Roy, Am. Mineral. **53**, 1929 (1968)
65. D.B. Rogers, J.L. Gillson, T.E. Gier, Solid State Commun. **5**, 263 (1967)
66. P. Toulmin III, P.B. Barton Jr., Geochim. Cosmochim. Acta **28**, 641 (1964)
67. A.J. Ellis, W.A.J. Mahon, Geochim. Cosmochim. Acta **28**, 1323 (1964)
68. R.A. Laudise, in *Progress in Inorganic Chemistry*, ed. by F. Albert Cotton, vol. 3 (Interscience, New York, 1962), p. 1
69. R.A. Laudise, J.W. Nielsen, Solid State Phys. **12**, 149 (1961)
70. S.A. Wood, Chem. Geol. **88**, 99 (1990)
71. E.L. Shock, Orig. Life Evol. Biosph. **20**, 331 (1990)
72. P.M. Dove, D.A. Crerar, Geochim. Cosmochim. Acta **54**, 955 (1990)
73. A. Michard, Geochim. Cosmochim. Acta **53**, 745 (1989)
74. J.C.I.V. Tanger, H.C. Helgeson, Am. J. Sci. **288**, 19 (1988)
75. B.M. Lok, C.A. Messina, R.L. Patton, R.T. Gajek, T.R. Cannan, E.M. Flanigen, J. Am. Chem. Soc. **106**, 6092 (1984)
76. E.B. Watson, T.M. Harrison, Earth Planet. Sci. Lett. **64**, 295 (1983)
77. E. Tani, M. Yoshimura, S. Somiya, J. Am. Ceram. Soc. **66**, 11 (1983)
78. S.T. Wilson, B.M. Lok, E.M. Flanigen, (Union Carbide Corp., USA). Application: EP, 108 pp (1982)
79. H. Ohmoto, A.C. Lasaga, Geochim. Cosmochim. Acta **46**, 1727 (1982)
80. G. Perego, M. Taramasso, B. Notari, (Snamprogetti SpA, Italy). Application: BE, 18 pp (1981)
81. S. Miyata, Clays Clay Miner. **28**, 50 (1980)
82. R.L. Penn, J.F. Banfield, Geochim. Cosmochim. Acta **63**, 1549 (1999)
83. W.-J. Li, E.-W. Shi, W.-Z. Zhong, Z.-W. Yin, J. Crystal. Growth. **203**, 186 (1999)
84. P. Feng, X. Bu, G.D. Stucky, Nature (London) **388**, 735 (1997)
85. C.J. Barbe, F. Arendse, P. Comte, M. Jirousek, F. Lenzmann, V. Shklover, M. Gratzel, J. Am. Ceram. Soc. **80**, 3157 (1997)
86. O.M. Yaghi, H. Li, J. Am. Chem. Soc. **117**, 10401 (1995)
87. B.L. Cushing, V.L. Kolesnichenko, C.J. O'Connor, Chem. Rev. **104**, 3893 (2004)
88. C.N.R. Rao, F.L. Deepak, G. Gundiah, A. Govindaraj, Progr. Solid State Chem. **31**, 5 (2003)
89. B. Liu, H.C. Zeng, J. Am. Chem. Soc. **125**, 4430 (2003)
90. L.E. Greene, M. Law, J. Goldberger, F. Kim, J.C. Johnson, Y. Zhang, R.J. Saykally, P. Yang, Angew. Chem. **42**, 3031 (2003). International Edition
91. C.S. Cundy, P.A. Cox, Chem. Rev. **103**, 663 (2003)
92. X. Wang, Y. Li, J. Am. Chem. Soc. **124**, 2880 (2002)
93. S. Inagaki, S. Guan, T. Ohsuna, O. Terasaki, Nature **416**, 304 (2002)
94. H. Zhang, X.-J. Lv, Y.-M. Li, Y. Wang, J.-H. Li, ACS Nano **4**, 380 (2010)
95. C.-Y. Sun, S.-X. Liu, D.-D. Liang, K.-Z. Shao, Y.-H. Ren, Z.-M. Su, J. Am. Chem. Soc. **131**, 1883 (2009)
96. B. Liu, E.S. Aydil, J. Am. Chem. Soc. **131**, 3985 (2009)

97. S. Zhu, Q. Meng, L. Wang, J. Zhang, Y. Song, H. Jin, K. Zhang, H. Sun, H. Wang, B. Yang, Angew. Chem. Int. Ed. **52**, 3953 (2013)
98. Q. Xiang, J. Yu, M. Jaroniec, Chem. Soc. Rev. **41**, 782 (2012)
99. Q. Xiang, J. Yu, M. Jaroniec, J. Am. Chem. Soc. **134**, 6575 (2012)
100. J. Jiang, K. Zhao, X. Xiao, L. Zhang, J. Am. Chem. Soc. **134**, 4473 (2012)
101. X.-C. Dong, H. Xu, X.-W. Wang, Y.-X. Huang, M.B. Chan-Park, H. Zhang, L.-H. Wang, W. Huang, P. Chen, ACS Nano **6**, 3206 (2012)
102. M.M. Lencka, R.E. Riman, Chem. Mater. **5**, 61 (1993)
103. W.L. Suchanek, R.E. Riman, Ceram. Sci. Technol. **3**, 63 (2012)
104. H. Hayashi, Y. Hakuta, Materials **3**, 3794 (2010)
105. M. Rajamathi, R. Seshadri, Curr. Opin. Solid State Mater. Sci. **6**, 337 (2002)
106. S.M. Gupta, M. Tripathi, Cent. Eur. J. Chem. **10**, 279 (2012)
107. G. Garnweitner, M. Niederberger, J. Am. Ceram. Soc. **89**, 1801 (2006)
108. M. Niederberger, G. Garnweitner, Chem. Eur. J. **12**, 7282 (2006)
109. M. Niederberger, G. Garnweitner, J. Ba, J. Polleux, N. Pinna, Int. J. Nanotechnol. **4**, 263 (2007)
110. M. Niederberger, G. Garnweitner, J. Buha, J. Polleux, J. Ba, N. Pinna, J. Sol-Gel Sci. Technol. **40**, 259 (2006)
111. M. Niederberger, G. Garnweitner, N. Pinna, G. Neri, Progr. Solid State Chem. **33**, 59 (2006)
112. A. Chemseddine, T. Moritz, Eur. J. Inorg. Chem. **235**, 235 (1999)
113. B. Tan, Y. Wu, J. Phys. Chem. B **110**, 15932 (2006)
114. C. Sun, H. Li, H. Zhang, Z. Wang, L. Chen, Nanotechnology **16**, 1454 (2005)
115. H. Toraya, M. Yoshimura, S. Somiya, J. Am. Ceram. Soc. **66**, 148 (1983)
116. M. Yoshimura, S. Somiya, Mater. Chem. Phys. **61**, 1 (1999)
117. Y. Zheng, Y. Cheng, Y. Wang, F. Bao, L. Zhou, X. Wei, Y. Zhang, Q. Zheng, J. Phys. Chem. B **110**, 3093 (2006)
118. Z.-s. Hong, Y. Cao, J.-f. Deng, Mater. Lett. **52**, 34 (2002)
119. C.L. Lu, J.G. Lv, L. Xu, X.F. Guo, W.H. Hou, Y. Hu, H. Huang, Nanotechnology **20**, 215604/1 (2009)
120. Y.V. Kolen'ko, K.A. Kovnir, I.S. Neira, T. Taniguchi, T. Ishigaki, T. Watanabe, N. Sakamoto, M. Yoshimura, J. Phys. Chem. C **111**, 7306 (2007)
121. G.H. Du, Q. Chen, P.D. Han, Y. Yu, L.M. Peng, Phys. Rev. B. Condens. Matter Mater. Phys. **67**, 035323/1 (2003)
122. A. Magrez, E. Vasco, J.W. Seo, C. Dieker, N. Setter, L. Forro, J. Phys. Chem. B **110**, 58 (2006)
123. J.W. Liu, G. Chen, Z.H. Li, Z.G. Zhang, Int. J. Hydrogen Energ. **32**, 2269 (2007)
124. Y. Li, X. Duan, H. Liao, Y. Qian, Chem. Mater. **10**, 17 (1998)
125. M. Niederberger, N. Pinna, J. Polleux, M. Antonietti, Angew. Chem. Int. Ed. **43**, 2270 (2004)
126. T. Adschiri, K. Kanazawa, K. Arai, J. Am. Ceram. Soc. **75**, 1019 (1992)
127. K. Byrappa, K.M.L. Rai, M. Yoshimura, Environ. Technol. **21**, 1085 (2000)
128. B. Zhao, L. Lin, D. He, J. Mater. Chem. A. Mater. Energ. Sustain. **1**, 1659 (2013)
129. H. Cheng, J. Ma, Z. Zhao, L. Qi, Chem. Mater. **7**, 663 (1995)
130. G.-S. Kim, Y.-S. Kim, H.-K. Seo, H.-S. Shin, Korean J. Chem. Eng. **23**, 1037 (2006)
131. Y. Xu, X. Fang, J. Xiong, Z. Zhang, Mater. Res. Bull. **45**, 799 (2010)
132. S. Kaewgun, C.A. Nolph, B.I. Lee, L.-Q. Wang, Mater. Chem. Phys. **114**, 439 (2009)
133. Y. Wu, H.-M. Liu, B.-Q. Xu, Z.-L. Zhang, D.-S. Su, Inorg. Chem. **46**, 5093 (2007)
134. S. Yin, Y. Aita, M. Komatsu, J. Wang, Q. Tang, T. Sato, J. Mater. Chem. **15**, 674 (2005)
135. J. Liu, W. Qin, S. Zuo, Y. Yu, Z. Hao, J. Hazard. Mater. **163**, 273 (2009)
136. G. Melcarne, L. De Marco, E. Carlino, F. Martina, M. Manca, R. Cingolani, G. Gigli, G. Ciccarella, J. Mater. Chem. **20**, 7248 (2010)
137. X. Zhang, X. Ge, C. Wang, Crystal Growth Design **9**, 4301 (2009)
138. B.-M. Wen, C.-Y. Liu, Y. Liu, New J. Chem **29**, 969 (2005)
139. K. Das, S.K. Panda, S. Chaudhuri, J. Crystal Growth **310**, 3792 (2008)

140. B. Santara, P.K. Giri, Mater. Chem. Phys. **137**, 928 (2013)
141. L. Jiang, M. Yang, S. Zhu, G. Pang, S. Feng, J. Phys. Chem. C **112**, 15281 (2008)
142. Y. Zhang, Y. Li, J. Phys. Chem. B **108**, 17805 (2004)
143. P.D. Cozzoli, L. Manna, M.L. Curri, S. Kudera, C. Giannini, M. Striccoli, A. Agostiano, Chem. Mater. **17**, 1296 (2005)
144. S. Biswas, S. Kar, S. Chaudhuri, J. Phys. Chem. B **109**, 17526 (2005)
145. H. Zhang, L. Wang, H. Xiong, L. Hu, B. Yang, W. Li, Adv. Mater. **15**, 1712 (2003)
146. S. Huang, Appl. Phys. B **84**, 323 (2006)
147. Y. Li, Y. Ding, Z. Wang, Adv. Mater. **11**, 847 (1999)
148. X.-H. Li, J.-X. Li, G.-D. Li, D.-P. Liu, J.-S. Chen, Eur. J. Chem. A **13**, 8754 (2007)
149. H. Cao, G. Wang, S. Zhang, X. Zhang, D. Rabinovich, Inorg. Chem. **45**, 5103 (2006)
150. M. Salavati-Niasari, M.R. Loghman-Estarki, F. Davar, Chem. Eng. J. **145**, 346 (2008)
151. Y. Yin, A.P. Alivisatos, Nature **437**, 664 (2005)
152. Y. Xie, Y. Qian, W. Wang, S. Zhang, Y. Zhang, Science **272**, 1926 (1996)
153. L. Grocholl, J. Wang, E.G. Gillan, Chem. Mater. **13**, 4290 (2001)
154. A.P. Purdy, Chem. Mater. **11**, 1648 (1999)
155. K. Sardar, C.N.R. Rao, Adv. Mater. **16**, 425 (2004)
156. K. Biswas, K. Sardar, C.N.R. Rao, Appl. Phys. Lett. **89**, 132503 (2006)
157. S.V. Bhat, K. Biswas, C.N.R. Rao, Solid State Commun. **141**, 325 (2007)
158. B. Mazumder, P. Chirico, A.L. Hector, Inorg. Chem. **47**, 9684 (2008)
159. F. Xu, Y. Xie, X. Zhang, S. Zhang, X. Liu, X. Tian, Inorg. Chem. **43**, 822 (2003)
160. S. Wei, J. Lu, W. Yu, Y. Qian, J. Appl. Phys. **95**, 3683 (2004)
161. Y.-D. Li, X.-F. Duan, Y.-T. Qian, L. Yang, M.-R. Ji, C.-W. Li, J. Am. Chem. Soc. **119**, 7869 (1997)
162. S. Gao, J. Lu, Y. Zhao, N. Chen, Y. Xie. Eur. J. Inorg. Chem. **2003**, 1822 (2003)
163. S. Wei, J. Lu, W. Yu, H. Zhang, Y. Qian, Chem. Lett. **33**, 386 (2004)
164. B. Hu, K. Wang, L. Wu, S.-H. Yu, M. Antonietti, M.-M. Titirici, Adv. Mater. **22**, 813 (2010)
165. M.-M. Titirici, M. Antonietti, N. Baccile, Green Chem. **10**, 1204 (2008)
166. M.M. Titirici, A. Thomas, M. Antonietti, Adv. Funct. Mater. **17**, 1010 (2007)
167. M.-M. Titirici, M. Antonietti, Chem. Soc. Rev. **39**, 103 (2010)
168. Y. Fang, D. Gu, Y. Zou, Z. Wu, F. Li, R. Che, Y. Deng, B. Tu, D. Zhao, Angew. Chem. Int. Ed. **49**, 7987 (2010)
169. W.Z. Wang, J. Y. Huang, Z. F. Ren, Langmuir, **21**, 751 (2004)
170. W.Z. Wang, B. Poudel, J.Y. Huang, D.Z. Wang, S. Kunwar, Z.F. Ren, Nanotechnology **16**, 1126 (2005)
171. J. Qiu, W. Shen, R. Yu, B. Yao, Chem. Lett. **37**, 644 (2008)
172. J.L.C. Rowsell, O.M. Yaghi, Angew. Chem. Int. Ed. **44**, 4670 (2005)
173. J.-R. Li, R.J. Kuppler, H.-C. Zhou, Chem. Soc. Rev. **38**, 1477 (2009)
174. M.K. Carpenter, T.E. Moylan, R.S. Kukreja, M.H. Atwan, M.M. Tessema, J. Am. Chem. Soc. **134**, 8535 (2012)
175. J. Lee, O.K. Farha, J. Roberts, K.A. Scheidt, S.T. Nguyen, J.T. Hupp, Chem. Soc. Rev. **38**, 1450 (2009)
176. W.J. Rieter, K.M. Taylor, H. An, W. Lin, J. Am. Chem. Soc. **128**, 9024 (2006)
177. A.C. McKinlay, R.E. Morris, P. Horcajada, G. Férey, R. Gref, P. Couvreur, C. Serre, Angew. Chem. Int. Ed. **49**, 6260 (2010)
178. R.C. Huxford, J. Della Rocca, W. Lin, Curr. Opin. Chem. Biol. **14**, 262 (2010)
179. J. Rocha, L.D. Carlos, F.A.A. Paz, D. Ananias, Chem. Soc. Rev. **40**, 926 (2011)
180. M. Sadakiyo, T. Yamada, H. Kitagawa, J. Am. Chem. Soc. **131**, 9906 (2009)
181. K.M.L. Taylor-Pashow, J.D. Rocca, Z. Xie, S. Tran, W. Lin, J. Am. Chem. Soc. **131**, 14261 (2009)
182. K.M.L. Taylor, A. Jin, W. Lin, Angew. Chem. Int. Ed. **47**, 7722 (2008)
183. K.M.L. Taylor, W.J. Rieter, W. Lin, J. Am. Chem. Soc. **130**, 14358 (2008)
184. W.J. Rieter, K.M.L. Taylor, W. Lin, J. Am. Chem. Soc. **129**, 9852 (2007)

185. Y. Chen, H. Chen, D. Zeng, Y. Tian, F. Chen, J. Feng, J. Shi, ACS Nano **4**, 6001 (2010)
186. C.M. Niemeyer, Angew. Chem. **40**, 4128 (2001)
187. P.V. Kamat, J. Phys. Chem. B **106**, 7729 (2002)
188. T. Mousavand, S. Ohara, M. Umetsu, J. Zhang, S. Takami, T. Naka, T. Adschiri, J. Supercrit. Fluid. **40**, 397 (2007)
189. W.C.W. Chan, S. Nile, Science. **281**, 2016 (1998)
190. A. Singhal, G. Skandan, A. Wang, N. Glumac, B.H. Kear, R.D. Hunt, Nanostruct. Mater. **11**, 545 (1999)
191. W. Posthumus, P.C.M.M. Magusin, J.C.M. Brokken-Zijp, A.H.A. Tinnemans, R. van der Linde, J. Colloid Interface Sci. **269**, 109 (2004)
192. B. Shahmoradi, K. Byrappa, A. Maleki, J. Mater. Sci. Eng. A **3**, 50 (2013)
193. T. Adschiri, Chem. Lett. **36**, 1188 (2007)
194. H. Cai, X. An, J. Cui, J. Li, S. Wen, K. Li, M. Shen, L. Zheng, G. Zhang, X. Shi, ACS Appl. Mater. Interfaces **5**, 1722 (2013)
195. K. Namratha, K. Byrappa, J. Supercrit. Fluid. **79**, 251 (2013)
196. D. Voltzke, S. Gablenz, H.P. Abicht, R. Schneider, E. Pippel, J. Woltersdorf, Mater. Chem. Phys. **61**, 110 (1999)